PLOS GENETICS

RESEARCH ARTICLE

Conserved chromatin regulators control the transcriptional immune response to intracellular pathogens in *Caenorhabditis elegans*

Eillen Tecle[1,2], Paaramitha Warushavithana[3], Samuel Li[3], Michael J. Blanchard[1], Crystal B. Chhan[1], Theresa Bui[1], Ryan S. Underwood[1], Malina A. Bakowski[1], Emily R. Troemel[1,*], Vladimir Lažetić[1,3,*]

1 Department of Cell and Developmental Biology, School of Biological Sciences, University of California, San Diego, La Jolla, California, United States of America, **2** Department of Microbiology and Immunology, Medical College of Wisconsin, Milwaukee, Wisconsin, United States of America, **3** Department of Biological Sciences, Columbian College of Arts and Sciences, The George Washington University, District of Columbia,Washington, United States of America

* vladimir.lazetic@gwu.edu (VL); etroemel@ucsd.edu (ERT)

OPEN ACCESS

Citation: Tecle E, Warushavithana P, Li S, Blanchard MJ, Chhan CB, Bui T, et al. (2025) Conserved chromatin regulators control the transcriptional immune response to intracellular pathogens in Caenorhabditis elegans. PLoS Genet 21(4): e1011444. https://doi.org/10.1371/journal.pgen.1011444

Editor: Javier E. Irazoqui, University of Massachusetts Medical School, UNITED STATES OF AMERICA

Received: September 30, 2024

Accepted: February 24, 2025

Published: April 7, 2025

Data availability statement: All relevant data are within the manuscript and its Supporting Information files.

Funding: This work was funded by NIH grants AG052622, GM114139, and AI176639 and NSF grant 2301657 awarded to E.R.T., the American Heart Association postdoctoral

Abstract

Robust transcriptional responses are critical for defense against infection. However, unrestrained immune responses can cause negative impacts such as damaging inflammation and slowed development. Here, we find that a class of transcriptional regulators previously associated with regulation of development in *Caenorhabditis elegans*, is also involved in repressing immune responses. Specifically, through forward genetics, we find that loss of *lin-15B* leads to constitutive expression of Intracellular Pathogen Response (IPR) genes. *lin-15B* encodes a transcriptional repressor with a conserved THAP domain that is associated with the DRM chromatin remodeling complex that regulates *C. elegans* development. We show that *lin-15B* mutants have increased resistance to natural intracellular pathogens, and the induction of IPR genes in *lin-15B* mutants relies on the MES-4 histone methyltransferase. We extend our analyses to other DRM and NuRD chromatin remodeling factors, as well as SUMOylation histone modifiers, showing that a broad range of chromatin-related factors can repress IPR gene expression. Altogether these findings suggest that conserved chromatin regulators may facilitate development in part by repressing damaging immune responses against intracellular pathogens.

Author summary

In this study, we show that transcriptional regulators, previously linked to development in *Caenorhabditis elegans*, also control immune responses. Through forward genetic screens, we found that loss of LIN-15B leads to constitutive activation of Intracellular Pathogen Response (IPR) genes. LIN-15B is functionally associated with the DREAM chromatin remodeling complex, and its loss enhances resistance to intracellular

award 19POST34460023 and The George Washington University Facilitating Fund Award to V.L., and NIGMS/NIH Institutional Research and Academic Career Development Award K12GM068524 to E.T. The funders had no role in study design, data collection and analysis, decision to publish, or preparation of the manuscript.

Competing interests: The authors have declared that no competing interests exist.

pathogens. This immune response depends on the MES-4 histone methyltransferase. We also discovered that other chromatin regulators, including NuRD and SUMOylation factors, similarly repress IPR gene expression, highlighting a new role in immunity for these conserved regulators of development.

Introduction

Innate immune responses are induced by host pattern recognition receptors (PRRs) that detect pathogen-associated molecular patterns (PAMPs), leading to downstream transcriptional activation [1]. One such PAMP is double-stranded RNA in the cytosol generated by RNA virus replication, which is sensed by mammalian cells using PRR RIG-I-like receptors. RIG-I-like receptors are cytosolic sensors that activate transcriptional induction of type-I interferon (IFN-I) ligands, including IFN-α and IFN-β [2–5]. These secreted IFN-I ligands bind to and activate IFN-I receptors on neighboring cells, leading to a systemic IFN-I immune response [5]. This response is crucial for defense against intracellular pathogens, but inappropriate IFN-I response activation can lead to developmental defects and damage due to inflammation [6–13].

Regulation of transcriptional responses involves not only transcription factors that recruit RNA polymerase to promoters, but also chromatin regulators that allow transcription factors to access regulatory regions of genes to promote transcription [14,15]. For example, the transcription factor IRF3 functions downstream of RIG-I-like receptors to induce early IFN-I ligand transcription [4], acting together with the SWI/SNF (Switch/Sucrose Non-Fermentable) complex, which is a chromatin remodeling complex that facilitates the binding of IRF3 to DNA to activate IFN-I ligand expression [16]. SWI/SNF was originally identified in yeast, and is just one of many conserved chromatin remodeling complexes that regulate transcription [17,18]. There is much to be learned about how such conserved chromatin regulators control immune gene expression, and the downstream impacts from perturbing these regulators, particularly in a whole-animal context.

Recently, there have been similarities described in the IFN-I response, and a transcriptional immune response in the nematode *Caenorhabditis elegans* called the Intracellular Pathogen Response (IPR) [7]. The IPR is induced by two types of intracellular pathogens that infect the *C. elegans* intestine in the wild: 1) species in the *Nematocida* genus of the Microsporidia phylum, which are obligate intracellular fungi, and 2) the Orsay virus, which is a single-stranded, positive-sense RNA virus [19–22]. *C. elegans* detects viral RNA replication products from the Orsay virus using a PRR called DRH-1, which, similar to other RIG-I-like receptors, uses tandem caspase activation and recruitment domains (2CARD) to induce a downstream transcriptional program [7,23–25]. The IPR promotes resistance to both microsporidia and Orsay virus infections, and comprises an immune response distinct from those mounted against extracellular bacterial infections. Thus, similar to the anti-viral IFN-I response in mammals, the IPR is a transcriptional response in *C. elegans* that provides defense against intracellular pathogens.

While the IPR promotes protection against intracellular pathogens, its activation can come at the cost of impaired organismal health in the absence of infection, similar to the overactivation of the IFN-I response [7,21,22,26]. For example, mutations in the *C. elegans* gene *pals-22* (from the *pals* gene family of unknown biochemical function) lead to constitutive IPR gene expression as well as increased resistance to infection by intracellular pathogens [21,22]. However, *pals-22* mutants display slowed growth, shortened lifespan, and signs of neuronal dysfunction [21,22]. These phenotypes can be reversed by a mutation in the downstream

positive regulator *pals-25*, which activates IPR gene expression in a *pals-22* mutant background [22,27]. This *pals-22/pals-25* module appears to act as an OFF/ON switch for IPR gene expression separately from DRH-1 activation of the IPR, and separately from another *pals* gene module comprised of *pals-17/pals-20/pals-16* identified through forward genetic screens for regulation of IPR transcription [22,26–28]. Similar to *pals-22* mutants, *pals-17* mutants have constitutive IPR gene expression and increased resistance against intracellular pathogens but impaired development [26].

While several genes in *C. elegans* like *pals-22/25* and *pals-17/16/20* have been shown to regulate development, IPR gene expression and resistance to infection [22,26,27,29], we know relatively little about downstream factors that mediate transcriptional induction, such as the direct regulators of IPR gene transcription. For example, while DRH-1 is a homolog of RIG-I-like receptors, *C. elegans* lacks homologs for several factors acting downstream of these receptors, such as the transcription factor IRF3. Instead, an RNAi screen in *C. elegans* identified the bZIP transcription factor ZIP-1 to be acting downstream of DRH-1, as well as downstream of other IPR triggers like microsporidia infection and *pals-22* mutations [30]. ZIP-1 promotes the expression of *pals-5*, which is commonly used as a reporter gene for IPR induction. Altogether, ZIP-1 is responsible for activating about 1/3 of IPR genes and promotes resistance to intracellular pathogens [30]. However, the transcription factor responsible for inducing *zip-1*-independent IPR genes is unknown, and there is much to be learned about how transcriptional regulators such as chromatin remodeling complexes and histone modifiers may affect IPR transcription.

Here we performed two independent forward genetic screens that both converged on the chromatin regulator LIN-15B as a new negative regulator of the IPR. LIN-15B is a THAP-domain (Thanatos-associated protein domain) protein and is functionally associated with the chromatin remodeling DRM complex (DREAM complex in mammals), which plays a key role in transcriptional repression during development. Our findings revealed that *lin-15B* functions upstream of the gene *mes-4*, which encodes an H3K36 methyltransferase histone modifier crucial for chromatin remodeling [31]. Importantly, we show that together with its activation of the IPR, loss of LIN-15B provides enhanced protection against infection with both the Orsay virus and *Nematocida parisii* microsporidia. LIN-15B, along with DRM complex genes, is part of the broader Synthetic Multivulva (SynMuv) family of developmental genes, which also includes Nucleosome Remodeling and Deacetylase complex (NuRD) genes and genes involved in SUMOylation. By testing various members of the SynMuv family, we found that most SynMuv genes, including both chromatin remodelers and histone modifiers, negatively regulate the IPR. In summary, our findings revealed the involvement of different conserved chromatin remodeling and transcription-regulating complexes in modulating immunity against obligate intracellular pathogens, and raise the intriguing possibility that several of these factors may allow for normal development by repressing expression of innate immune genes.

RESULTS

Two independent genetic screens isolate DRM-associated protein LIN-15B as a novel negative regulator of the IPR

To uncover novel negative regulators of the IPR, we conducted two independent forward EMS mutagenesis screens using the *pals-5*p::GFP transcriptional IPR reporter. In both screens, we identified mutants with constitutive expression of *pals-5*p::GFP in the absence of infection. The first screen (33,504 haploid genomes screened) was performed in the *pals-22 pals-25* mutant background, which has wild-type levels of IPR expression and induction, due to loss

of both the IPR negative regulator *pals-22* and its downstream activator *pals-25*. The screen was performed in this genetic background in order to not identify new mutations of *pals-22*. Four mutants with constitutive *pals-5*p::GFP expression were isolated in this screen, one of which was the IPR negative regulator *pals-17*, as previously published [26]. The second screen was performed in a wild-type genetic background (26,000 haploid genomes screened) and nine mutants with constitutive *pals-5*p::GFP expression were isolated in this screen, including the IPR negative regulator *pnp-1*, as previously published [29].

After performing complementation analysis among mutants from these two screens, we found that one mutant from each of the two screens failed to complement each other for the phenotype of constitutive *pals-5*p::GFP expression, suggesting that they may encode mutations in the same gene. Whole genome sequencing analyses revealed that both of these mutants had mutations in the gene *lin-15B*. The mutant from the first screen contained three missense mutations in the second exon of *lin-15B*, leading to the following amino acid changes: Ala56Thr, His157Gln, and Ala168Thr, and was designated the *jy76* allele of *lin-15B*. The mutant from the second screen had a single missense mutation in the seventh exon of *lin-15B*, resulting in a Cys1142Tyr substitution in the protein sequence, and was designated the *jy86* allele of *lin-15B* (Figs 1 and S1). This mutation is located in the region that encodes a THAP domain, protein motif with similarity to the DNA-binding domain of P element transposase [32], which is important for LIN-15B function as a transcriptional regulator [33]. To investigate whether these mutations behave as loss-of-function alleles for canonical *lin-15B* phenotypes, we tested whether we could induce the characteristic SynMuv phenotype in the isolated mutants. *lin-15B* belongs to the SynMuvB group, which exhibits this phenotype when SynMuvA genes are downregulated. We thus exposed *lin-15B(jy86)* mutants to RNAi against *smo-1* (a SynMuvA gene) and assessed their progeny. Here we found that most *smo-1* RNAi treated animals developed one or more protruding vulvas, a defect indicative of the simultaneous loss of SynMuvA and SynMuvB genes (S2 Fig). No such changes were observed in control RNAi animals.

To determine whether endogenous *pals-5* mRNA levels are increased in *lin-15B* mutants and to identify the tissues in which *pals-5* mRNA is expressed, we performed single-molecule fluorescence in situ hybridization (smFISH) analysis. While *pals-5* mRNA was mostly undetectable in wild-type animals, *lin-15B* mutants exhibited numerous *pals-5* mRNA puncta (S3 Fig). Additionally, *pals-5* mRNA expression appeared to be specific to intestinal cells in this mutant, even though *pals-5* can be expressed more widely in other genetic backgrounds, such as when *pals-22/25* signaling is perturbed. However, only a subset of intestinal cells expressed *pals-5* puncta in *lin-15B* mutants, and the pattern of expression seemed to be stochastic, as different intestinal cells showed *pals-5* mRNA expression in different animals. To ensure that the selective expression was not an artifact of partial stain penetration, we stained the samples with DAPI, which stained all nuclei, indicating that the permeabilization process was effective. Additionally, we quantified the number of *pals-5* mRNA puncta in the first and second intestinal rings and found significantly higher *pals-5* expression in *lin-15B* mutants compared to the control strain (S3 Fig and S1 Table). In summary, *lin-15B* mutants had not only *pals-5* reporter induction but also endogenous *pals-5* mRNA induction.

lin-15B mutants have increased immunity against natural intracellular pathogens of the intestine

Because IPR induction has previously been linked to increased resistance to intracellular pathogens [22,26,29,30], we tested whether *lin-15B* mutants exhibit enhanced immunity against these pathogens. First, we examined the response to *N. parisii*, which is the most

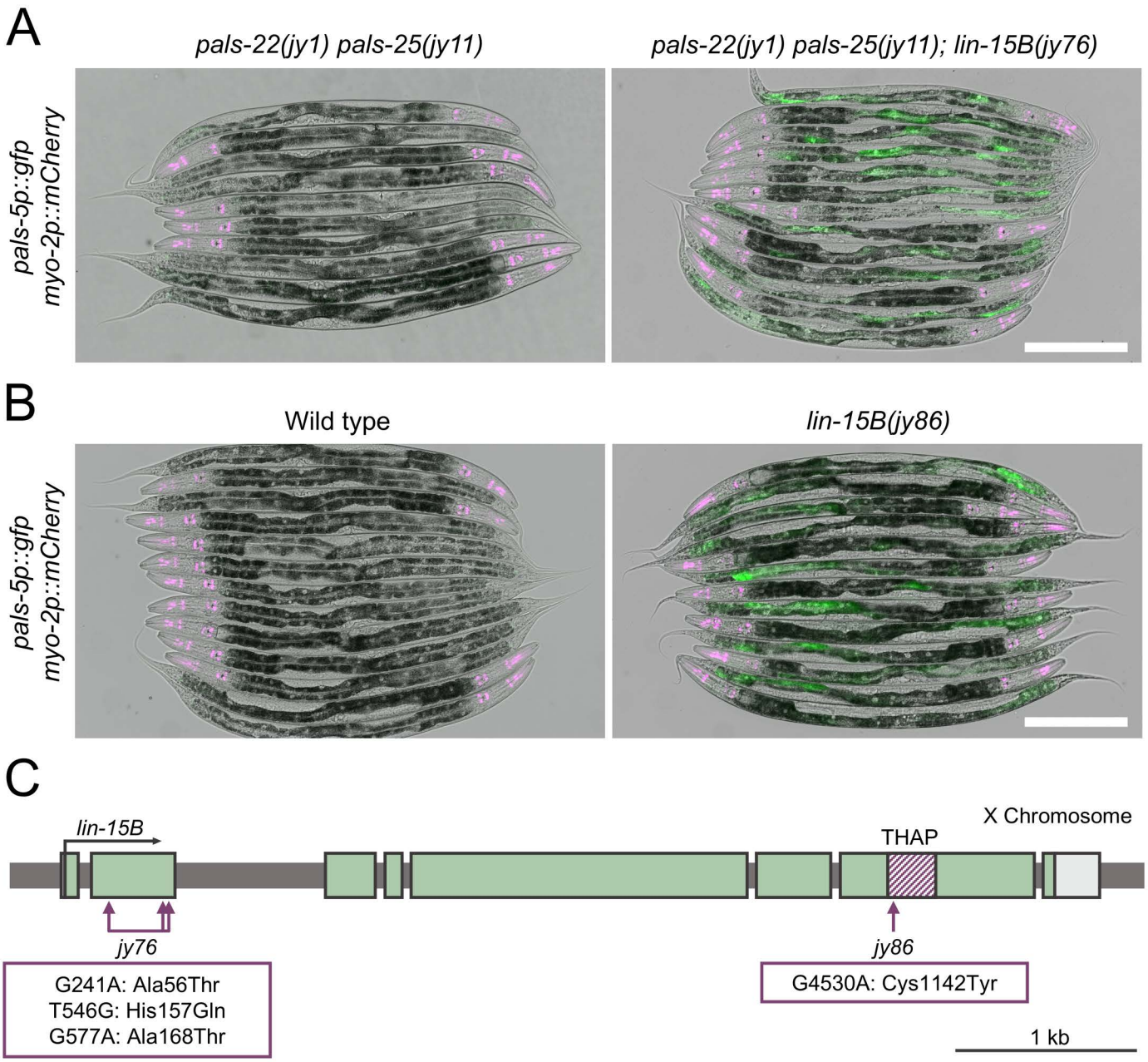

Fig 1. ***lin*-15B is a negative regulator of *pals*-5p::GFP expression.** (A, B) Mutants isolated from two independent forward genetic screens in *pals-22 pals-25* double mutant (A) and wild-type backgrounds (B) show increased expression of *pals-5*p::GFP reporter (shown in green). *myo-2*p::mCherry co-injection marker is shown in magenta. Green, magenta and DIC channels were merged. Scale bar = 200 μm. (C) *lin-15B* gene structure. *lin-15B* exons are indicated with green boxes, UTRs are shown in light gray, region encoding THAP domain is indicated with striped magenta box. Horizontal arrow shows the direction of transcription. Vertical arrows indicate positions of point mutations in alleles *jy76* and *jy86*.

https://doi.org/10.1371/journal.pgen.1011444.g001

commonly found microsporidia species infecting *C. elegans* in the wild, and has tropism for the intestine [28,34]. To determine whether *lin-15B* mutants exhibit increased pathogen tolerance, we performed a killing assay and found that *lin-15B(jy86)* mutants survived significantly longer after infection with *N. parisii* compared to wild-type animals (Fig 2A and S1 Table). Of note, loss of *lin-15B* has been previously reported to decrease lifespan [35], so the improved

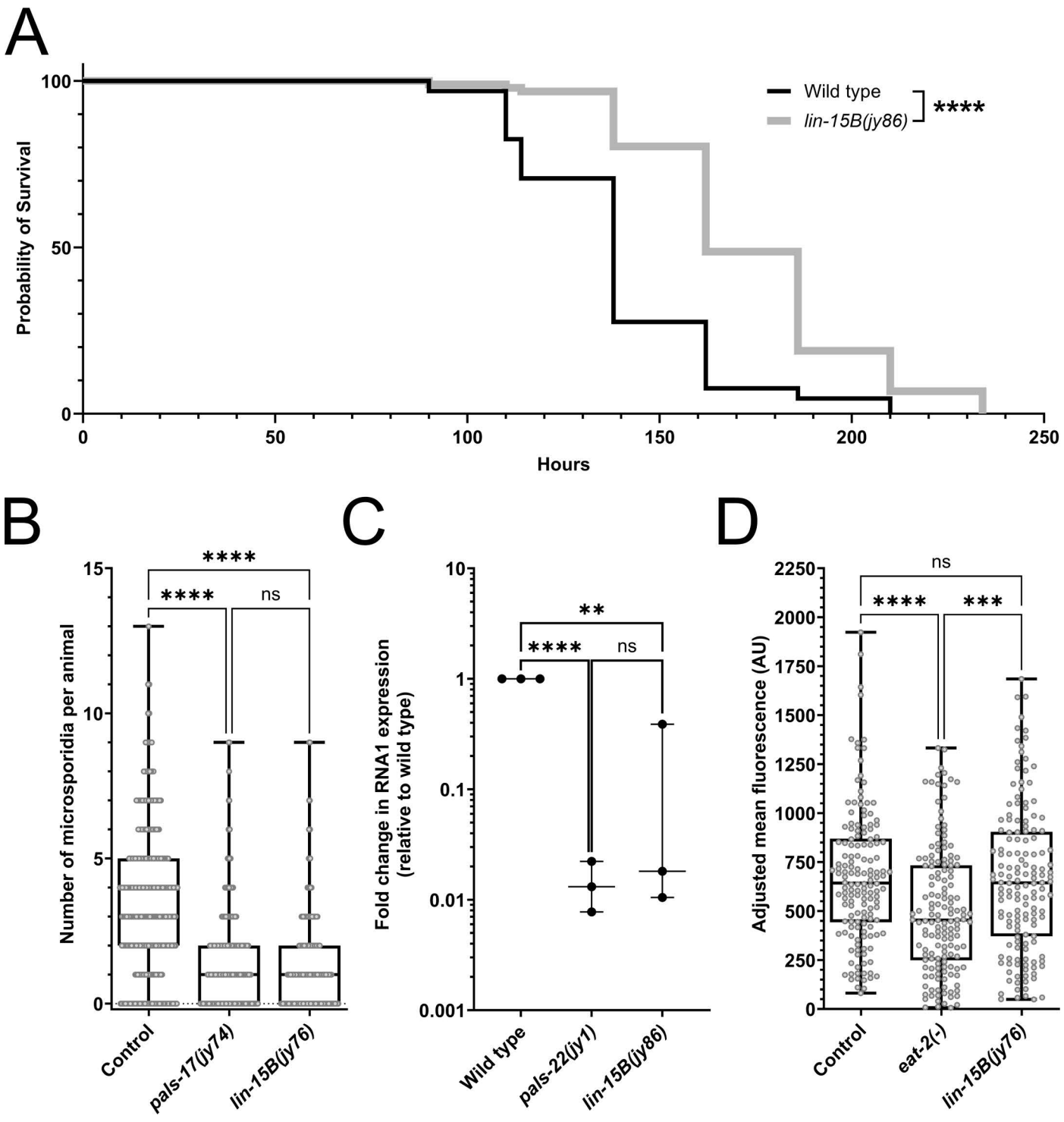

Fig 2. IPR activation in *lin-15B* mutants provides protection against natural intracellular pathogens of the intestine. (A) Survival of wild-type and *lin-15B(jy86)* mutants after infection with *N. parisii*. The Mantel-Cox test was used to determine *p*-values: **** $p < 0.0001$. (B) *N. parisii* pathogen load quantified at 3 hpi as number of sporoplasms per animal. (C) qRT-PCR analysis of Orsay virus pathogen load. Each experimental replicate is shown by a dot. A one-tailed t-test was used to calculate *p*-values; asterisks represent a significant difference between the labeled sample and the wild-type control; **** $p < 0.0001$; ** $p < 0.01$; ns = no significant difference. (D) Box-and-whisker plot of adjusted bead fluorescence levels per animal. The *eat-2(ad465)* mutant strain is a feeding-defective control. AU = arbitrary units. (B, D) Box lines represent median values, while box edges mark the 25th and 75th percentiles. Whiskers extend to the minimum and maximum values. Three experimental replicates were performed. Gray circles indicate individual values for each animal; 100 (B) and 50 (D) animals were analyzed per strain per replicate. The Kruskal-Wallis test was used to determine *p*-values: **** $p < 0.0001$; *** $p < 0.001$; ns = no significant difference.

https://doi.org/10.1371/journal.pgen.1011444.g002

survival of *lin-15B* mutants after *N. parisii* infection cannot be attributed to an increased lifespan. To test if *lin-15B* animals are also more resistant to microsporidia infection (i.e. have lower pathogen load), we infected the strain in which *jy76* allele was isolated (with *pals-5p::gfp* reporter; negative control), *pals-17* mutants from the same screen (positive control), and *lin-15B(jy76)* mutants with *N. parisii* spores and quantified the pathogen load at the sporoplasm (early parasite cell) stage across these three backgrounds. Here we found that *lin-15B* mutants had a lower number of sporoplasms in the intestine per animal, compared to the negative control, showing similar resistance to the *pals-17* mutants. Thus, *lin-15B* appears to regulate immunity against *N. parisii* infection (Fig 2B and S1 Table).

Next, we investigated whether *lin-15B* mutants had increased resistance to infection with the Orsay virus, which is also a natural pathogen of *C. elegans* with tropism for the intestine. Using a feeding method to introduce pathogen infection [26], we infected wild-type animals (negative control), *pals-22* mutants (positive control), and *lin-15B(jy86)* mutants with the Orsay virus and measured Orsay RNA1 levels using qRT-PCR. Here our results showed a significant decrease in viral RNA in *lin-15B* mutants, comparable to the reduction seen in *pals-22* mutants, again supporting the model that *lin-15B* regulates immune responses against intracellular pathogens (Fig 2C and S1 Table).

To rule out the possibility that differences in food intake or excretion might explain the variations in pathogen load in *lin-15B* mutants, we measured intestinal accumulation of fluorescent beads in the original strain used in the screen, *eat-2(-)* eating-defective control and *lin-15B* mutants. Here we found that *lin-15B* mutants accumulated beads similarly to the original strain, suggesting that the enhanced immunity in *lin-15B* mutants is not due to altered feeding behavior (Fig 2D and S1 Table). In conclusion, our data indicate that the loss of *lin-15B* promotes immunity against natural intracellular pathogens of the *C. elegans* intestine.

Loss of LIN-15B induces expression of multiple IPR genes, dependent on histone methyltransferase MES-4

To determine the extent of IPR gene expression regulated by *lin-15B*, we analyzed two previously published transcriptomic data sets for *lin-15B* loss-of-function mutant animals [33,36]. While variables such as the specific conditions used in these prior studies could substantially influence these comparisons, we found that 69 out of 80 canonical IPR genes (86.25%) were induced in at least one analyzed data set, with 42 IPR genes (52.5%) being induced in both data sets (including *pals-5*) (S4A Fig and S2 Table). Of the 30 IPR genes previously reported as ZIP-1-dependent, 28 were identified as LIN-15B-dependent in at least one dataset. Similar to previously identified mutants with constitutive upregulation of the IPR, like *pals-22* and *pals-17* mutants [21,26], both *lin-15B* mutant alleles we isolated displayed developmental delay. We found that a synchronized population of *lin-15B* mutants takes 10 hours longer than control strains to progress from the first larval stage (L1) to the fourth larval stage (L4) when grown at 20°C (58 h vs. 48 h). Due to the presence of a THAP domain in LIN-15B, which is a DNA-binding motif involved in regulating gene transcription and chromatin structure [37,38], we hypothesized that this protein might directly bind to IPR genes whose expression it regulates. However, previous ChIP-seq studies of LIN-15B [33] indicate that it only directly binds to five IPR genes (*pals-26*, *pals-27*, *Y6E2A.5*, *fbxa-75,* and *Y41C4A.11*) (S3 Table), suggesting that it might indirectly regulate transcription of the majority of IPR genes, again with the caveat that these studies may have been performed with different conditions than the studies here.

LIN-15B is a protein associated with the dimerization partner, RB-like, E2F, and multivulval class B (DREAM) complex, called DRM in *C. elegans* [33]. Thus, we refer to LIN-15B as a DRM-AP for DRM-associated protein. The retinoblastoma (Rb) ortholog in *C. elegans* is named LIN-35 and is associated with development [33,39–44]. Our analysis of published

transcriptomic data from *lin-35* mutants [36] indicates that the majority of IPR genes (62.5%; 50/80) are functionally repressed by LIN-35 (S4B Fig and S2 Table). Among the 30 IPR genes previously identified as ZIP-1-dependent, 25 were found to also depend on LIN-35 in the analyzed dataset. LIN-35 is a transcriptional repressor that, among other functions, prevents expression of histone methyltransferase MES-4 in somatic tissues, including the intestine [36,45,46]. Interestingly, MES-4 is important for the expression of many genes that are repressed by LIN-35 [36]. We analyzed if *lin-35*-dependent IPR genes are *mes-4*-dependent and found that 70% (35/50) of those genes or 43.75% (35/80) of all IPR genes require *mes-4* for their transcriptional upregulation in *lin-35* mutant background (S4B Fig and S2 Table). Therefore, our analysis suggests that *lin-35* predominantly suppresses the induction of IPR genes by downregulating or inhibiting *mes-4* expression.

Previous ChIP-seq studies indicate that *mes-4* is one of the genes bound by LIN-15B (S3 Table) [33], potentially suggesting a mechanism for IPR gene regulation. Although *mes-4* mRNA expression was not upregulated in *lin-15B* mutants from the same study [33], an earlier transcriptomic study of *lin-15B* mutants reported an increase in *mes-4* mRNA levels (S2 and S3 Tables) [36]. The same ChIP-seq dataset [33], indicates that LIN-15B binds to *pals-17* and *pals-22*, two negative regulators of the IPR (S3 Table). However, mRNA expression of these genes was not reported to be significantly altered in *lin-15B* mutants (S2 Table) [33,36], perhaps due to low expression level of these two genes.

To address whether *lin-15B,* like *lin-35,* requires *mes-4* for IPR induction, we first analyzed *pals-5*p::GFP expression in *lin-15B(jy76)* mutants on control and *mes-4* RNAi plates. We observed a substantial reduction in GFP expression following *mes-4* RNAi treatment, suggesting that, similar to *lin-35* mutants, IPR induction in *lin-15B* mutants is *mes-4*-dependent (Fig 3A). To analyze the regulation of endogenous IPR mRNA expression by *lin-15B* and *mes-4*, we performed qRT-PCR on our *lin-15B(jy86)* allele, as well as the canonical loss-of-function *lin-15B(n744)* allele, under control or *mes-4* RNAi conditions (Fig 3B). First, we observed a significant induction of IPR gene expression in both *lin-15B* alleles, providing further support that *lin-15B(jy86)*, like *lin-15B(n744)* is a loss-of-function allele, and that multiple IPR genes are induced when LIN-15B is lost. Next, we found that *mes-4* RNAi reduced IPR gene expression in these mutants compared to control RNAi, suggesting that *mes-4* functions downstream of *lin-15B* during IPR activation. While the reduction was not back to wild-type levels of expression, this partial effect may be due to the maternal effect of *mes-4*, or incomplete knock-down by RNAi (*mes-4* is an essential gene). Altogether, these results support the model that loss of *lin-15B* induces many IPR genes in a manner dependent on *mes-4*.

Loss of multiple chromatin regulators (SynMuv genes) induces the IPR

lin-15B and *lin-35* are members of the SynMuv family of genes that regulate vulval development as well as other developmental processes through their involvement in transcriptional regulation and chromatin remodeling (Fig 4A) [47–49]. Using an RNAi approach, we investigated whether the downregulation of other SynMuv genes also induces expression of the IPR. We analyzed *pals-5*p::GFP reporter expression following RNAi of different SynMuv genes in two different age categories – L1 to L3 stage and L4 to adult stage. We classified GFP expression as none, weak, and strong GFP. L4440 control vector and *pals-17* RNAi were used as negative and positive controls for IPR induction, respectively.

We found that downregulation of multiple SynMuv genes from different functional subfamilies induces the expression of the IPR reporter (Fig 4B and 4C, and S1 Table). In general, stronger induction was observed in the older age category of the animals. Our results suggest that SynMuv genes encoding various components of the DRM complex and DRM-APs

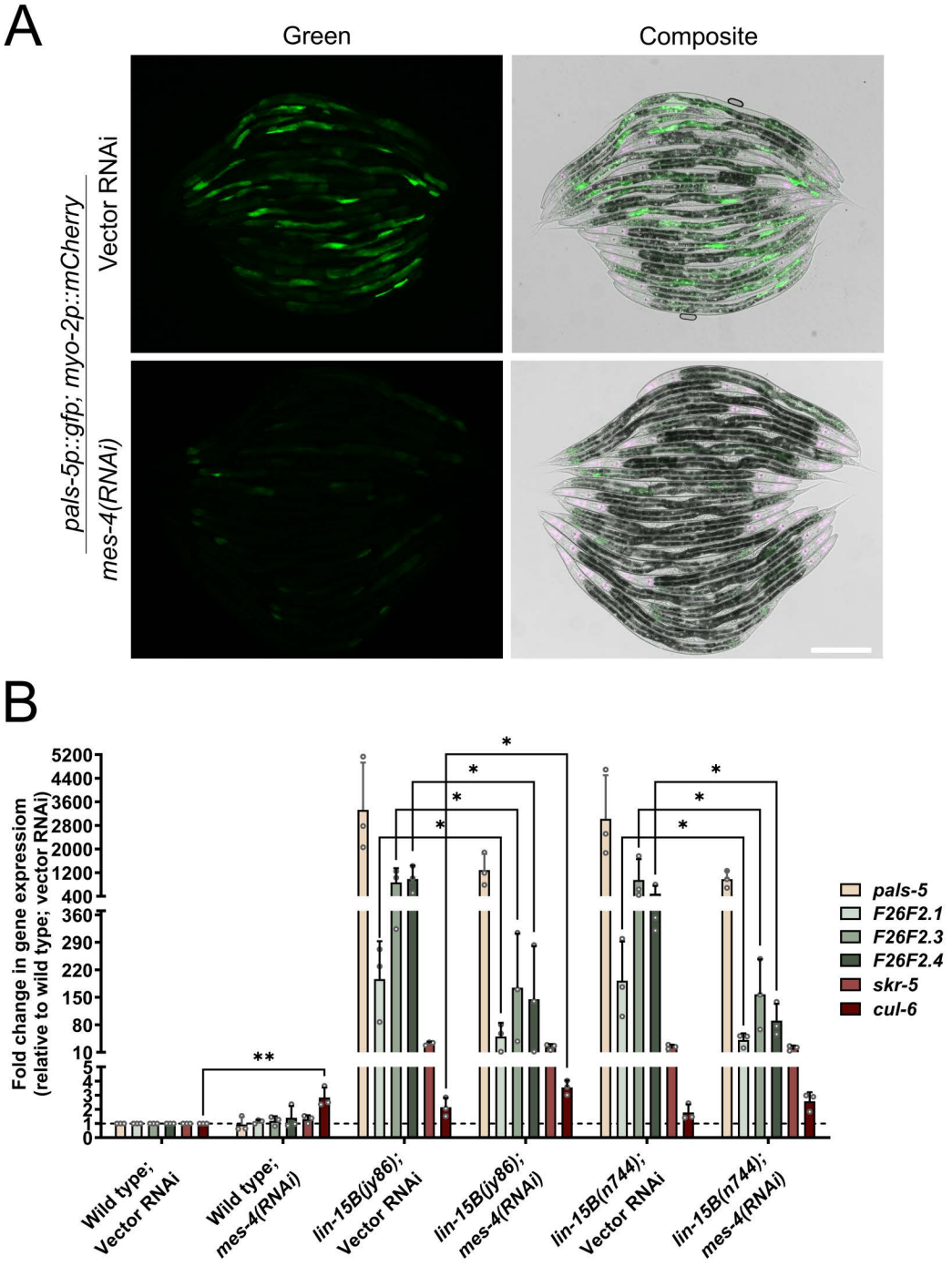

Fig 3. IPR gene expression in *lin-15B* mutants is dependent on *mes-4*. (A) *pals-5*p::GFP expression in *lin-15B* mutants is reduced following *mes-4* RNAi treatment. *pals-5*p::GFP is shown in green; *myo-2*p::mCherry co-injection marker is shown in magenta. Magenta, green and DIC channels were merged in the composite images. Scale bar = 200 μm. (B) qRT-PCR expression analysis of a subset of IPR genes in *lin-15B(jy86)* and *lin-15B(n744)* mutants treated with vector and *mes-4* RNAi. Fold change in gene expression is shown relative to wild-type animals on vector RNAi. Three independent experimental replicates are shown; gray circles indicate values for each replicate; error bars are SD. A one-tailed t-test was used to calculate *p*-values; asterisks represent a significant difference between two samples; ** $\boldsymbol{p} < 0.01$; * $\boldsymbol{p} < 0.05$; *p*-values higher than 0.05 are not labeled (analysis was performed only within the same genetic backgrounds).

https://doi.org/10.1371/journal.pgen.1011444.g003

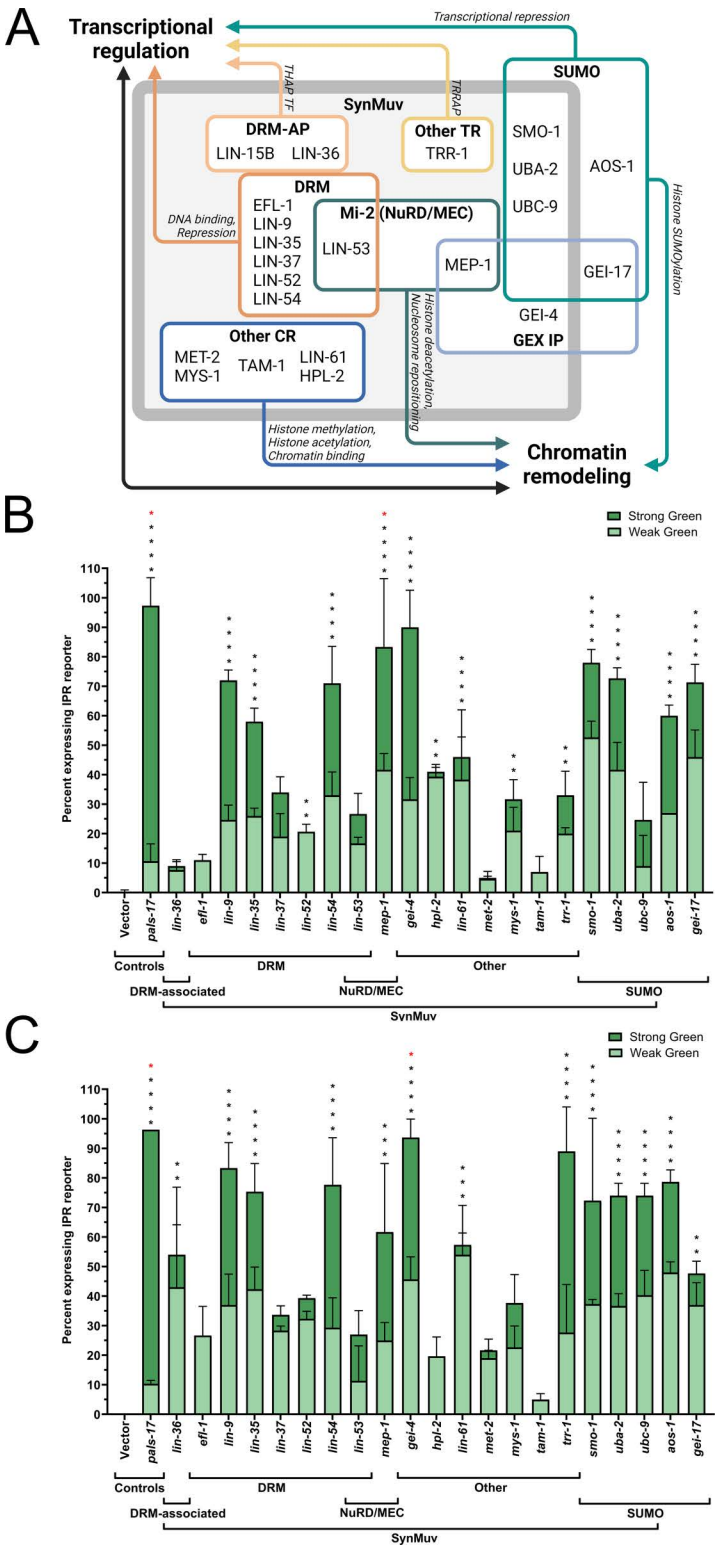

Fig 4. Multiple chromatin regulators in the SynMuv class negatively regulate *pals-5*p::GFP expression. (A) Model depicting functional complexes in the SynMuv gene/protein family and their roles in transcriptional regulation and chromatin remodeling. Abbreviations: DRM – DP, Rb, Myb; DRM AP – DRM-Associated Proteins; TR – Transcription Regulators; NuRD – Nucleosome Remodeling and Deacetylase; GEX – Gut on EXterior; IP – Interacting Protein; CR – Chromatin Remodeler. Created with BioRender.com. (B, C) Downregulation of different SynMuv components

induces *pals-5*p::GFP expression in L1-L3 (B) and L4-Adult developmental stages (C). Error bars are shown separately for the "Strong GFP" and "Weak GFP" categories and represent SD. Statistical analyses were performed on the total number of green animals (both weak and strong GFP expression), with all values compared to the control vector RNAi. Black asterisks represent *p*-values calculated using ordinary one-way ANOVA test with Holm-Šídák multiple comparison test; red asterisks represent *p*-values calculated using the Kruskal-Wallis test; **** $p < 0.0001$; *** $p < 0.001$; ** $p < 0.01$; * $p < 0.05$; *p*-values higher than 0.05 are not labeled.

https://doi.org/10.1371/journal.pgen.1011444.g004

negatively regulate the IPR. The DRM complex is composed of several key components: a repressive transcription factor EFL-1 protein with its dimerization partner DPL-1, an Rb-like pocket protein LIN-35, and a core MuvB complex consisting of five subunits – LIN-9, LIN-37, LIN-52, LIN-53, and LIN-54 [47,50]. Interestingly, we observed varying levels of GFP expression across different DRM RNAi treatments. For example, downregulation of *lin-54*, *lin-35*, and *lin-9* caused the strongest induction of the IPR reporter, while *efl-1* downregulation resulted in a more modest effect (Fig 4B and 4C, and S1 Table). Additionally, downregulation of *lin-36*, which encodes a DRM-AP with a THAP domain, led to low induction of *pals-5*p::GFP in early larval stages, but its expression increased in L4 and adult animals (Fig 4B and 4C, and S1 Table).

To explore whether these differences stem from RNAi efficacy or actual functional differences between the genes, and to gain further insights into the expression changes of multiple IPR genes, we analyzed transcriptomics data from previous studies on several DRM mutants [33]. We found that, in addition to *lin-15B* and *lin-35* mutants, a subset of IPR genes is upregulated upon the loss of other DRM genes, such as *dpl-1* (10%, 8/80) and *lin-37* (57.5%, 46/80) (S5 Fig and S4 Table). However, no significant upregulation of IPR gene expression was observed in *efl-1* mutants. Likewise, no IPR gene induction was present in *lin-36* mutants (S5 Fig and S4 Table). These findings align with our RNAi studies, where we observed stronger *pals-5*p::GFP expression in *lin-35(RNAi)* and *lin-37(RNAi)* animals, and lower GFP expression in *efl-1(RNAi)* and *lin-36(RNAi)* animals (Fig 4B and 4C, and S1 Table). Taken together, these data suggest that different DRM components may have distinct roles in regulating IPR induction.

In our targeted RNAi screen, we also observed that components of complexes containing the Mi-2 nucleosome remodeler, NuRD and MEP, negatively regulate IPR reporter expression (Fig 4). Also *pals-5*p::GFP expression was robustly induced by RNAi against several other SynMuv genes, particularly by *gei-4* (encoding GEX Interacting protein) and *trr-1* (encoding TRRAP-like protein) knockdown (Fig 4). However, downregulation of *met-2* (encoding histone methyltransferase) and *tam-1* (Tandem Array expression Modifier; involved in ubiquitylation) had relatively weak or almost no effect on IPR reporter expression (Fig 4). We also analyzed available transcriptomics data for *met-2* mutants and found no induction of IPR gene expression in this genetic background (S4 Table). In summary, our results suggest that a subset of SynMuv genes play a role in IPR induction.

Loss of SUMOylation factors induces the expression of multiple IPR genes

Several genes encoding core SUMOylation components are also part of the SynMuv gene family [48,51]. SUMOylation is a conserved post-translational modification process that alters the function of many substrate proteins and is closely linked to transcriptional regulation and chromatin remodeling [52–55]. In *C. elegans*, this process involves the stepwise attachment of a small protein, SUMO (or SMO-1), to a substrate via a cascade of enzymatic activities involving E1 (composed of AOS-1 and UBA-2), E2 (UBC-9), and E3 complexes (GEI-17) [56,57]. In our targeted RNAi screen, we found that downregulation of all three SynMuv genes from

the SUMO family – *smo-1*, *uba-2*, and *ubc-9* – induced the expression of the *pals-5*p::GFP reporter (Figs 4B, 4C, and 5A and S1 Table). We also discovered that SUMOylation genes *aos-1* and *gei-17*, not previously annotated as SynMuv, also negatively regulate the IPR (Fig 4B and 4C, and S1 Table).

To assess whether SUMOylation affects the endogenous expression of *pals-5* and several other IPR genes, we conducted qRT-PCR analysis. We observed a substantial increase in IPR gene expression following RNAi treatments targeting *smo-1*, *uba-2*, and *aos-1*, with modest or low IPR induction following the downregulation of other SUMOylation genes (Fig 5B and S1 Table). Our previous yeast two-hybrid analysis demonstrated that the positive IPR regulator PALS-25 physically interacts with three SUMOylation components involved in IPR regulation: SMO-1, UBC-9, and GEI-17 [27]. To explore this connection further, we conducted a similar analysis using the IPR activator PALS-20 as bait and identified a subset of shared interactors with PALS-25. Notably, all three SUMOylation proteins were found to interact with both PALS-20 and PALS-25 (Fig 5C and S5 Table). In summary, our findings suggest a novel role for SUMOylation in regulating the transcription of IPR genes, possibly by modulating the activity of PALS proteins as positive regulators of the IPR.

Discussion

Mechanisms of chromatin remodeling during the activation of transcriptional immune responses are not well understood. In this study, we identified several chromatin remodeling and transcriptional repressor complexes that act as negative regulators of the IPR in *C. elegans* (Fig 6). First, through an unbiased approach, we discovered that *lin-15B* functions as a repressor of the IPR. We demonstrated that the loss of *lin-15B* confers tolerance and resistance to obligate intracellular pathogens. Our small-scale targeted RNAi screen revealed that multiple genes from the SynMuv family, which are functionally related to *lin-15B*, also negatively regulate the IPR. Mechanistically, our data suggest that *lin-15B* operates upstream of *mes-4*, which is necessary for IPR induction in this context (Fig 6).

Although LIN-15B lacks a direct mammalian homolog [58], it features a well-conserved THAP domain, which is frequently found in transcriptional regulators [33,59]. While this domain is not essential for DNA binding by LIN-15B, it is crucial for its functionality [33]. LIN-15B, along with another SynMuv THAP-domain protein, LIN-36, is functionally linked to the conserved DRM complex, which globally represses gene expression and inhibits cell cycle progression in differentiated cells [33,60,61]. The DRM complex uses these THAP proteins to regulate its genomic targets; however, LIN-15B and LIN-36 govern different subsets of DRM-regulated genes via distinct mechanisms [33]. By analyzing the expression of the IPR fluorescent reporter following *lin-36* depletion, we observed some induction of the GFP, especially in older animals, suggesting that roles of *lin-15B* and *lin-36* might somewhat overlap in this context. However, based on transcriptomic data, *lin-36* does not seem to function as an IPR repressor [33].

As for the role of DRM complex components in IPR regulation, we found that some components of this complex have stronger effect on IPR regulation than others. This result could mean that not all components of DRM complex are involved in transcriptional repression of the IPR and that a subset of DRM genes might form a distinct complex involved in immune regulation. For example, we found that *efl-1* RNAi treatment had a minor effect on *pals-5*p::GFP expression induction and that none of the IPR genes are induced in an *efl-1* mutant background. Interestingly, EFL-1 is essential for repressing LIN-35 targets shared with LIN-36, but it is not required for repressing those shared with LIN-15B [33]. Alternatively, certain

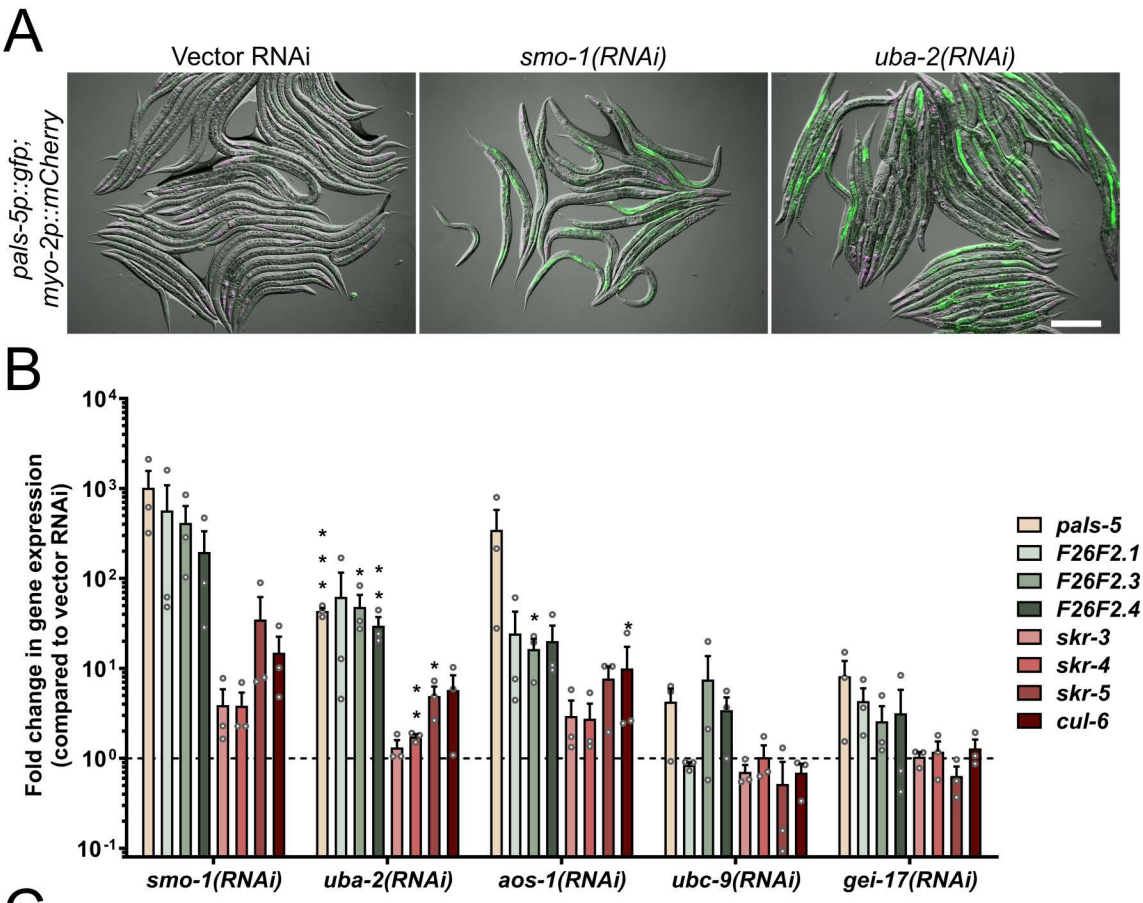

Gene name	PBS
adah-1	A
istr-1	A
pals-19	B
ubxn-3	B
spat-3	C
grdn-1	D
lin-13	D
pals-16	D
rpn-6.1	D
rrf-1	D
tnsl-1	D
ZK1053.4	D

Gene name	PBS PALS-20	PBS PALS-25	Gene name	PBS PALS-20	PBS PALS-25
gei-17	A	A	*pro-1*	D	D
hrde-4	B	C	*rad-26*	A	A
hrpk-2	A	B	*set-6*	B	A
mep-1	A	A	***smo-1***	D	B
npp-9	D	D	*szy-4*	D	D
picd-1	B	D	***ubc-9***	B	A

Gene name	PBS
blos-2	B
C16A11.4	B
pals-22	B
rab-1	B
C27C12.1	D
gadr-3	D
him-1	D
imb-1	D
mdt-29	D
pqn-94	D
rpn-1	D
unc-22	D
unc-42	D

Fig 5. Depletion of SUMOylation components induces IPR gene expression. (A) *smo-1* and *uba-2* RNAi treatments induce *pals-5*p::GFP expression in intestine. Green, magenta and DIC channels were merged. *pals-5*p::GFP is shown in green; *myo-2*p::mCherry co-injection marker is shown in magenta. Scale bar = 200 μm. (B) qRT-PCR analysis of representative IPR genes following downregulation of major SUMOylation components. Gene expression shown as the mean fold changes relative to the wild-type control in mixed stage population. Three independent experimental replicates are shown; gray circles indicate values for each replicate; error bars are

SD. A one-tailed t-test was used to calculate *p*-values; asterisks represent a significant difference between the labeled sample and the vector control; *** $p < 0.001$; ** $p < 0.01$; * $p < 0.05$; *p*-values higher than 0.05 are not labeled. (C) Yeast two-hybrid analysis of PALS-20 and PALS-25 interactors, including SUMOylation proteins SMO-1, UBC-9 and GEI-17 (yellow). PBS: A = very high confidence in the interaction, **B** = high confidence in the interaction, **C** = good confidence in the interaction, **D** = moderate confidence in the interaction.

https://doi.org/10.1371/journal.pgen.1011444.g005

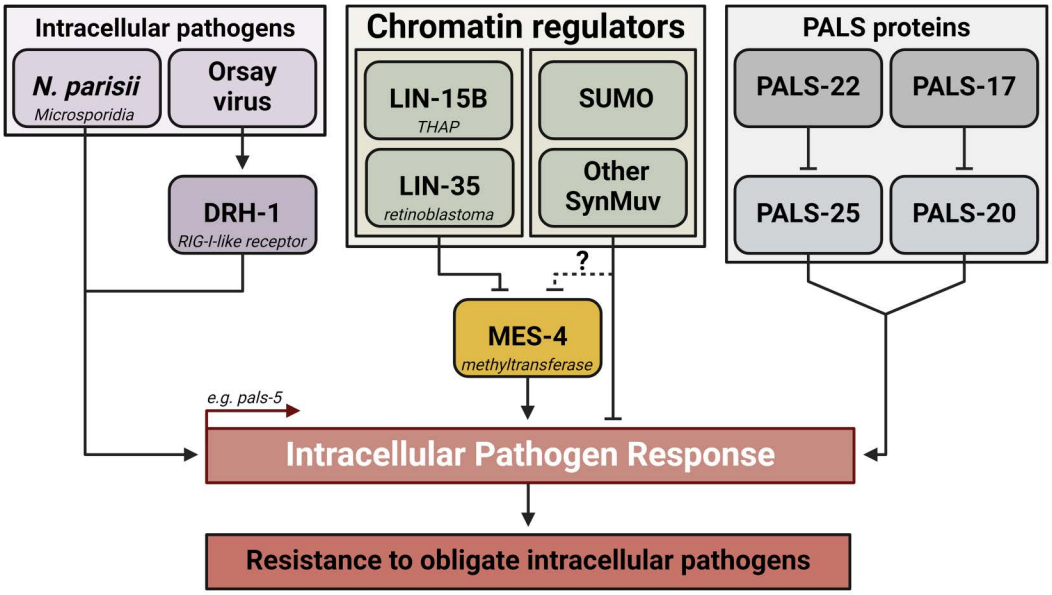

Fig 6. Model of IPR regulation by SynMuv proteins and MES-4. Created with BioRender.com.

https://doi.org/10.1371/journal.pgen.1011444.g006

components of the DRM complex might have redundant roles, and therefore downregulating a single subunit would not cause a drastic effect on IPR induction.

Analysis of previously published microarray, RNA-seq, and ChIP-seq datasets suggests that LIN-15B regulates the expression of most IPR genes but binds to DNA for only a few of them [33,36]. Additionally, LIN-15B binds to the *mes-4* gene and requires this gene for IPR reporter induction. MES-4 is a histone methyltransferase that catalyzes lysine 36 methylation on histone 3 [31,62], an epigenetic mark characteristic of transcriptionally accessible chromatin [63,64]. These regions may contain IPR genes, suggesting that LIN-15B might regulate IPR gene expression indirectly through the repression of MES-4. *mes-4* is a single homolog of three closely related mammalian genes Nsd1, Nsd2 and Nsd3 (Nuclear receptor-binding SET domain protein) [62]. MES-4 promotes transcription of germline genes and is most highly expressed in the germline [59,65]. Some DRM components (LIN-54/LIN54 and EFL-1/E2F) and MES-4 co-bind the same genomic targets in the germline, fine-tuning gene expression and allowing the proper development of the germline cells [66]. Interestingly, LIN-35 shows reduced binding in the germline, whereas, in somatic tissues, it directly binds to the promoter region of *mes-4* and represses its transcription [45]. Loss of *lin-35* leads to transcriptional upregulation of *mes-4* in the soma, initiating the germline fate in these tissues [36,45,46]. Future studies will investigate if similar changes occur during infection with obligate intracellular pathogens.

Our data demonstrate that *lin-15B* mutants have increased resistance to infection with the intestinal pathogens microsporidia and the Orsay virus. This finding aligns

with recent findings suggesting that the activity of SynMuvB genes is downregulated during Orsay virus infection [67], and with studies indicating that *lin-35* mutants confer maternally transferred immunity against microsporidia [68]. One possibility is that these pathogens may inhibit SynMuv components like LIN-35 and LIN-15B in intestinal cells to induce a less differentiated state, which is metabolically a more favorable environment for pathogen growth [69]. Notably, a comparative analysis of microsporidian genomes revealed that all examined species encode DP and E2F components of the DREAM complex but lack a *lin-35*/Rb ortholog [70]. It is intriguing to consider that microsporidia may have lost Rb from their genome while simultaneously inhibiting Rb in their host, converting intestinal cells into a more permissive environment for replication. A similar phenomenon has been observed in leprosy bacteria, where host cell de-differentiation enhances bacterial spread [71].

Because the loss of the *C. elegans* Rb ortholog, *lin-35*, leads to the upregulation of a gene set similar to those induced during microsporidia infection, it raises the possibility that the host recognizes DRM complex dysfunction as a signal associated with pathogen presence, triggering an immune response. This suggests that SynMuv proteins may have been evolutionarily selected as "guardees" frequently targeted by pathogens and are monitored by the immune system as infection signals. In this context, it parallels the Guard Hypothesis from plant and mammalian immunity [72–74], where immune receptors detect disruptions in key host proteins as a sign of infection. For example, the primary antiviral function of the DNA-binding protein MORC3 in mammalian cells is safeguarded by its secondary role in repressing IFN; thus, a virus that degrades MORC3 to evade its antiviral effects will unleash this secondary immune response [13].

A related hypothesis is that pathogen effectors modify chromatin as a strategy to evade the immune response. For example, the microsporidian *Encephalitozoon hellem* secretes EnP1 into the host's nucleus, inhibiting histone 2B monoubiquitylation and suppressing p53-mediated ferroptosis [75]. Furthermore, adenovirus counters host defenses through chromatin remodeling, with its early protein E1A forming a p300-e1a-RB1 complex that condenses chromatin, repressing host genes by redistributing histone modifications [76,77]. These chromatin changes could act as tripwires, triggering immune system activation. In fact, chromatin modifications are tightly linked to immune regulation, as nucleosome remodeling is essential for activating pathogen response genes and IFN-I-stimulated factors [78,79]. Additionally, Rb inhibits IFN-β production by deacetylating its promoter [80], while the NuRD complex downregulates STAT1 through histone deacetylation [81]. These insights underscore the critical role of chromatin regulators in fine-tuning immune responses and maintaining proper immune function.

Most of the genes we investigated belong to the SynMuvB class of SynMuv gene family, but our targeted RNAi screen also identified several genes previously classified as SynMuvA (*smo-1* and *uba-2*) and SynMuvC (*mys-1* and *ttr-1*) [48,62,82]. These three classes work in parallel pathways to repress inappropriate vulval cell fates [48]. Our results suggests that multiple SynMuv classes may be involved in immune regulation. Notably, while the SUMOylation genes *smo-1* and *uba-2* are categorized as SynMuvA, they exhibit functional characteristics of both SynMuvA and SynMuvB classes in vulval development [48]. Similarly, the SynMuvB gene *ubc-9* also displays SynMuvA-like functions in vulval development [48]. The remaining core SUMOylation components, AOS-1 and GEI-17, are not classified as SynMuv genes, yet we found that all SUMOylation genes negatively regulate the IPR. We hypothesize that, like other SynMuv genes, SUMOylation genes contribute to chromatin remodeling during IPR activation. This hypothesis aligns with the known role of SUMOylation in repressing the IFN-I response in mammals [83].

SUMOylation plays several crucial roles in different aspects of development [84,85]. Interestingly, mutations in other SynMuv genes also result in developmental abnormalities [86]. In this study, we observed delayed postembryonic development in *lin-15B* mutants. Given that prolonged activation of the IPR and IFN-I response has been linked to delayed development and developmental arrest [7,21,26], it is possible that the delayed development in SynMuv mutants may in part be due to immune system overactivation – an aspect that has not been previously explored. In conclusion, our study identified numerous genes involved in regulating innate immunity in *C. elegans*. Importantly, most of these genes are conserved in mammals. Given the regulatory similarities between the IPR and IFN-I response [7], it is possible that these genes retained their immunosuppressive functions across species.

Materials and methods

C. elegans strains

C. elegans strains were cultured on Nematode Growth Media (NGM) agar plates seeded with streptomycin-resistant *Escherichia coli* OP50-1 and grown at 20°C, unless otherwise specified [87]. The strains utilized in this study are listed in S6 Table.

Synchronization of *C.* elegans

C. elegans population synchronization was performed as described before [88]. In brief, gravid adult animals were washed off plates with M9 buffer and collected into 15 ml conical tubes. The tubes were centrifuged, and the supernatant was removed, leaving 3 ml of M9 buffer. 1 ml of bleaching solution (500 µl of 5.65–6% sodium hypochlorite and 500 µl of 5 M NaOH) was added, and the tubes were mixed until the adult animals were partially dissolved. The volume was brought up to 15 ml with M9 buffer to wash the released embryos. The tubes were immediately centrifuged, and the supernatant was removed. This washing step was repeated four times, and the embryos were resuspended in a final volume of 3 ml of M9 buffer. The embryos were then incubated at 20 °C with continuous rotation for 18–24 hours to allow them to hatch into L1 larvae.

Forward genetic screens and mapping of *lin-15B* alleles

The forward genetic screens and allele mapping were performed as previously described [26,29,89]. In brief, L4-stage animals carrying the *jyIs8[pals-5p::gfp, myo-2p::mCherry]* transgene (and *pals-22(jy1) pals-25(jy11)* mutations from the first screen, where the *jy76* allele was isolated, and wild-type animals from the second screen, where the *jy86* allele was isolated) were harvested from NGM plates using M9 buffer. The worms were then collected into 15 mL conical tubes, centrifuged, and the supernatant was discarded. Afterward, the worms were washed twice with M9 to remove residual bacteria. The pellet was resuspended in 4 ml of M9, and 25 µl of mutagen, ethyl methanesulfonate (EMS), was added. The worms were incubated at room temperature with continuous rotation for 4 hours. Post-incubation, the worms were centrifuged again, and the supernatant was discarded. They were washed twice more with M9 to remove the mutagen. The treated worms were then plated on 10 cm Petri dishes containing OP50-1 bacteria and incubated at room temperature for 2.5 hours to recover. Following this recovery period, mutagenized worms were transferred to fresh 10 cm Petri plates with OP50-1 bacteria and incubated at 20 °C. After 36 hours, the P0 animals were removed, and the F1 progeny continued to develop. After three days, F1 adults were bleached to synchronize their F2 progeny, which were then screened for *pals-5*p::GFP expression. The *jy86* allele was identified in the F2 population, while the *jy76* allele was identified in the F3 generation following

F2 bleaching. Approximately 33,500 and 26,000 haploid genomes were screened in the first and second screens, respectively. Isolated mutants were backcrossed six times to the original strains. Backcrossing to the original strains used in the screens revealed that the causative mutation is located on the X chromosome. In a complementation test, *jy76* and *jy86* failed to complement each other, suggesting they carry causative mutations in the same gene.

Genomic DNA was extracted from the original and mutant strains using the Qiagen Puregene Core Kit A and sent to BGI Genomics for whole genome sequencing. Data analysis was conducted using the Galaxy platform (https://usegalaxy.org). Read quality was evaluated with FastQC. Reads were aligned to the *C. elegans* reference genome (WBCel235.dna.toplevel.fa.gz) using Bowtie2 [90,91]. Genetic variants were detected with FreeBayes. Allelic variants were processed with VcfAllelicPrimitives to split allelic primitives into separate VCF lines. The VCF datasets for wild-type and mutants were compared using VCF-VCFintersect. Variants were filtered based on the criteria (QUAL > 30) & (DP ≥ 10) & (isHOM(Gen[0])) using SnpSift Filter [92], and the remaining variants were annotated with the SnpEff eff program [93].

The mutations in the *jy76* and *jy86* alleles were confirmed through Sanger sequencing (S1 Fig). Primers used to amplify the mutated regions are given in S7 Table. Although the presence of three point mutations within a 337-nucleotide region, including one T-to-G mutation instead of the typical G-to-A changes, is unusual for EMS mutagenesis, EMS has been reported to cause small deletions that may have been irregularly repaired in the *jy76* allele [94].

Imaging

For the analysis of *pals-5*p::GFP expression, animals were anesthetized with either 20 or 100 μM levamisole. They were then placed on agarose pads on glass slides and covered with cover slips. The samples were imaged using a Zeiss Axio Imager.M2 compound microscope with ZEN 3.8 software or a Zeiss Axio Imager.M1 compound microscope with Axio Vision 4.8.2 software. Image processing was performed using the FIJI software [95].

Single-molecule fluorescence in situ hybridization (smFISH)

Synchronized animals were placed on NGM plates seeded with OP50-1 bacteria and incubated at 20°C for 48 hours. After incubation, the animals were washed off the plates and fixed in 4% paraformaldehyde with PBST (phosphate-buffered saline containing 0.1% Tween 20) for 30 minutes at room temperature. Following fixation, the samples were incubated overnight at 4°C in 70% ethanol. For staining, 1 μM Quasar 670-conjugated *pals-5* smFISH probes (Biosearch Technologies) were used in a hybridization buffer containing 10% formamide, 2× SSC, 10% dextran sulfate, 2 mM vanadyl ribonucleoside complex, 0.02% RNase-free BSA, and 50 μg of *E. coli* tRNA. The samples were incubated overnight at 30°C in the dark. Afterward, they were washed with a buffer containing 10% formamide and 2x SSC at 30°C in the dark for 30 minutes. Vectashield with DAPI was then added to each sample, and the stained animals were transferred onto microscope slides, covered with glass coverslips, and imaged. Z-stack images of the region containing the anterior part of the intestine were acquired using a Zeiss Axio Imager.M1 compound microscope equipped with a 63x oil immersion objective and Axio Vision 4.8.2 software. Z stack processing into maximal projection images was performed using the FIJI software [95]. smFISH puncta quantification was performed using the StarSearch program (https://rajlab.seas.upenn.edu/resources). For the first intestinal ring, the anterior border was defined by the visible boundary between the pharynx and the intestine, while the posterior boundary was set at the midpoint between the DAPI-stained nuclei of the first and second intestinal rings [30]. For the third intestinal ring, the cell boundaries were determined by the

midpoint between the DAPI-stained nuclei of the second and third intestinal rings (anterior border) and between the third and fourth intestinal rings (posterior border).

N. parisii killing assay

N. parisii killing assay was performed as previously described [29]. Briefly, approximately 100 synchronized L1 worms were plated on 3.5 cm NGM plates with a mixture of 50 μl of 10X OP50-1 *E. coli* and 50,000 *N. parisii* spores. Four plates per strain were used per replicate, and the plates were incubated at 25 °C. The spore dosage was optimized to achieve a 50% killing rate in wild-type worms after 100 hours, testing doses of 25, 50, 75, and 100 thousand spores. After 66 hours, the worms were transferred to new 3.5 cm NGM plates containing OP50 without the pathogen, with 33 animals per strain per replicate. Animals were incubated at 25 °C and scored at least once daily. Death was determined by the absence of movement after three gentle touches with a metal pick. Animals that died at the edge of the plate due to desiccation were censored from the analysis. Three experimental replicates were performed. Data were analyzed using GraphPad Prism 10 Survival Tables, with dead animals assigned a value of "1" and censored animals a value of "0". Statistical analyses were performed using the Chi-square test and the Gehan-Breslow-Wilcoxon test, with significance indicated by **** $p < 0.0001$.

Microsporidia infection for pathogen load quantification

One million *N. parisii* spores were combined with 10 μl of 10x OP50-1 *E. coli*, along with 1,200 synchronized L1-stage *C. elegans*, and M9 buffer, bringing the total volume to 300 μl. This mixture was spread on 6 cm NGM plates, left to dry for 30 minutes at room temperature, and then incubated at 25 °C for 3 hours. Following incubation, the worms were collected using M9 buffer with 0.1% Tween 20, washed in PBST, and fixed in 4% paraformaldehyde for 45 minutes. The fixed worms were stained overnight at 46 °C using a Cal Fluor 610 red FISH probe, which specifically binds to *N. parisii* ribosomal RNA [96]. Imaging was performed with a Zeiss Axio Imager.M1 compound microscope with Axio Vision 4.8.2 software, and data were analyzed and statistically processed using GraphPad Prism 10 software.

Orsay virus infection and quantification of viral RNA1

Approximately 2,000 synchronized L1-stage worms were placed on 10 cm NGM plates seeded with *E. coli* OP50-1 for each strain. The plates were kept at 20°C for about 44 hours until the worms reached the L4 stage. A viral mixture was prepared by diluting 30 μl of the Orsay virus filtrate (1:10 in M9 buffer) and combining it with 150 μl of concentrated OP50-1 and 600 μl of M9 buffer. This mixture was added to 10 cm plates containing L4-stage worms, dried at room temperature, and incubated at 20°C for 24 hours. RNA was extracted using Tri-reagent (Molecular Research Center, Inc) and BCP phase separation reagent (Molecular Research Center, Inc), and converted to cDNA with the iScript cDNA synthesis kit (Bio-Rad). For qRT-PCR, iQ SYBR Green Supermix (Bio-Rad) was used along with primers specific to the Orsay virus RNA1 (S7 Table). Gene expression was normalized to *snb-1*, which remained constant under the tested conditions. Each sample was run in two technical replicates, and three independent experimental replicates were performed.

Bead-feeding assay

The bead feeding assay was performed as previously described [26]. Briefly, 1,200 synchronized L1-stage worms were combined with 6 μl of fluorescent beads (Fluoresbrite Polychromatic Red Microspheres, Polysciences Inc.), 25 μl of a 10X concentrated OP50-1 *E. coli*

solution, and M9 buffer to a total volume of 300 µl. This mixture was spread onto 6 cm NGM plates, allowed to air dry for 5 minutes, and incubated at 25°C. After a 5-minute incubation, plates were placed on ice. Worms were washed off the plates with ice-cold PBST, then fixed in 4% paraformaldehyde for 30 minutes. Following fixation, the samples were washed with PBST, and the worms were imaged using a Zeiss Axio Imager.M2 compound microscope with ZEN 3.8 software. Red fluorescence was quantified in the FIJI program [95], analyzing 50 worms per strain in each of three experimental replicates. Data were processed with GraphPad Prism 10.

Transcriptomics and ChIP-seq data analyses

Data were obtained from the publications referenced in the main text. Data overlap was analyzed using Multiple List Comparator software (https://molbiotools.com/listcompare.php). The gene name conversions were made using WormBase ParaSite Biomart (https://parasite.wormbase.org/biomart).

qRT-PCR analysis of IPR gene expression in *lin-15B* mutants

RNA interference (RNAi) by feeding was performed as previously described [97]. Briefly, overnight cultures of *E. coli* HT115 containing either control vector (L4440), *unc-22*, or *mes-4* RNAi clones were made. The cultures were seeded onto NGM plates containing 5 mM IPTG and 1 mM carbenicillin and allowed to grow at room temperature for 3 days. L4440 served as a negative control for IPR induction, and *unc-22* as a positive control for RNAi induction. N2, *lin-15B(jy86)*, and *lin-15B(n744)* animals were submitted to RNAi. For each biological replicate, L1 animals were synchronized by bleaching and seeded per plate as follows: 1000 N2, 3000 *lin-15B(jy86)*, and 3000 *lin-15B(n744)*, then grown to the L4 stage at 20°C. Two plates per condition were used for each experimental replicate, and three experimental replicates were performed. Plates of the same genotype and RNAi treatment were pooled for RNA extraction.

RNA from L4 animals was extracted using TRI reagent (Molecular Research Center, Inc.), 1-Bromo-3-chloropropane (Molecular Research Center, Inc.) and Direct-zol RNA Microprep Kit (Zymo). cDNA was generated using the iScript cDNA synthesis kit (Bio-Rad). qRT-PCR was performed using iQ SYBR green supermix (Bio-Rad) and gene-specific primers (S7 Table) on a BioRad CFX Connect real-time system. Each biological replicate was analyzed in technical duplicate and normalized to *snb-1*, a control gene that had no expression change in any condition. Statistical analysis was performed in Prism 10 using an unpaired, one-tailed student t-test, and a p-value < 0.05 was considered significantly different.

Targeted RNA interference screen

RNAi assays were conducted using the feeding method [98]. 23 distinct overnight cultures of HT115 *E. coli* RNAi strains were seeded onto RNAi plates (NGM plates supplemented with 5 mM IPTG and 1 mM carbenicillin) and incubated at room temperature for 3 days. L4440 served as a negative RNAi control, while *pals-17* RNAi was used as a positive control for inducing *pals-5*p::GFP expression. L4-stage *C. elegans* were transferred to RNAi plates and incubated at 20°C. After 48 and 72 hours, *pals-5*p::GFP expression was evaluated in the F1 progeny, with separate analysis for L1-L3 stage animals and L4-young adult stage animals. A total of 100 animals were analyzed per age group and per RNAi condition. Phenotypic analysis was performed using a Stereo Discovery V8 fluorescent microscope equipped with an X-Cite XYLIS XT720S illumination system. Data analysis was carried out using GraphPad Prism 10 software.

SUMO RNAi treatments and qRT-PCR analysis of IPR gene expression

RNA interference assays were performed using the feeding method [98]. Overnight cultures of *E. coli* were plated on RNAi plates (NGM plates supplemented with 5 mM IPTG and 1 mM carbenicillin) and incubated at room temperature for 24 hours. L4 animals were picked onto 3 10-cm seeded RNAi plates per strain (number of animals per plate: L4440 control vector RNAi – 12; *aos-1* RNAi – 20; *gei-17* – 18, *ubc-9* – 15; *smo-1* – 24) and incubated at 20 °C until majority of F1 progeny reached the L4 stage. RNA isolation was performed as previously described using Tri-reagent (Molecular Research Center, Inc) and BCP phase separation reagent (Molecular Research Center, Inc), and cDNA synthesis was performed using the iScript DNA synthesis kit (Bio-Rad) [26]. qRT-PCR was performed using iQ SYBR Green Supermix (Bio-Rad) with the CFX Connect Real-Time PCR Detection System (Bio-Rad). As a control, values were normalized to expression levels of the neuronal gene *snb-1*, which is not affected by IPR activation. Primer sequences are listed in S7 Table. Data analysis was performed through PRISM using the Pfaffl method. One-tailed t-tests were used to determine statistical significance between samples. Each sample was run in two technical replicates, and three independent experimental replicates were performed.

Yeast two-hybrid analysis

The yeast two-hybrid (Y2H) screen was carried out using the ULTImate Y2H cell-to-cell mating method (Hybrigenics Service, Evry, France), as previously described [27]. In brief, the coding sequence for PALS-20 was synthesized and inserted into the pB66 plasmid downstream of the Gal4 DNA-binding domain. This construct served as the bait to screen a *C. elegans* mixed-stage cDNA prey library, which was generated through random priming and cloned into the pP6 plasmid containing the Gal4 activation domain. The screen employed a haploid mating strategy, with one yeast sex type (mata) containing the bait and the other (matα) carrying the prey constructs [99]. In total, 79.8 million interactions were examined, yielding 279 clones that grew on selective media lacking tryptophan, leucine, and histidine. Prey fragments from the positive clones were PCR-amplified and sequenced at both 5' and 3' ends to identify the corresponding proteins using the NCBI GenBank database. The Predicted Biological Scores (PBS), which assess the reliability of bait-prey interactions, were explained previously [27,100] and are summarized for all identified interactions in S5 Table.

Supporting information

S1 Fig. Partial genomic sequences of *lin*-15B with mutations identified in the *jy76* and *jy86* alleles. (A, B) Wild-type and mutated nucleotides in *jy76* (A) and *jy86* (B) are shown on the positive strand, with mutated nucleotides highlighted in red boxes (uppercase letters). Surrounding sequences, including 500 nucleotides upstream and downstream, are displayed in gray boxes (lowercase letters).
(TIF)

S2 Fig. Downregulation of SynMuvA genes induces Synthetic Multivulva phenotype in *lin*-15B mutants. Representative images of developmental defects observed in *lin-15B(jy86)* mutants after exposure to *smo-1* RNAi. Enlarged insets provide a closer view of the vulval region for each corresponding full-body image. White arrows indicate normal vulvas, yellow arrows highlight protruding vulvas with normal localization, and blue arrows mark ectopic protruding vulvas. Scale bars: 200 μm (full-body images), 60 μm (insets).
(TIF)

S3 Fig. *pals*-5 mRNA expression is induced in intestinal cells in *lin*-15B mutants relative to control strain. (A) Representative Z-stack maximal projections of smFISH (left) and DAPI

staining (right) are shown. White arrows indicate regions with *pals-5* mRNA puncta, and yellow asterisks mark the expression of the pharyngeal marker *myo-2*p::mCherry. Scale bar = 50 μm. (B, C) Quantification of *pals-5* mRNA puncta in the first (B) and third (C) intestinal rings, n = 15 animals per sample. In the box-and-whisker plots, the line inside the box represents the median, the box bounds correspond to the 25th and 75th percentiles, and the whiskers extend from the box to the minimum and maximum values. *p*-values were calculated using a Mann-Whitney test; **** $p < 0.0001$.
(TIF)

S4 Fig. The majority of IPR genes are upregulated in *lin*-15B and *lin*-35 mutants and most of IPR genes upregulated in *lin*-35 mutants are dependent on *mes-4*. (A, B) *In silico* analysis of two previously published transcriptomic datasets for *lin-15B* (A) and *lin-35* mutants (B). IPR gene names that are underlined were previously reported to be ZIP-1-dependent. (B) The asterisk indicates a gene that was removed from the original list because it was not found among the genes upregulated in the *lin-35(-)* mutant.
(TIF)

S5 Fig. A subset of SynMuv genes regulate IPR gene expression. *In silico* analysis a previously published transcriptomic datasets. The numbers in parentheses indicate the count of upregulated genes in the annotated genetic backgrounds and IPR genes. Numbers in the intersecting cells represent the number of genes common to both datasets.
(TIF)

S1 Table. Data shown in graphs in main and supplementary figures.
(XLSX)

S2 Table. Comparative analysis of IPR genes and transcriptomic data for *lin-15*, *lin-35* and *mes-4*.
(XLSX)

S3 Table. Comparative analysis of IPR genes and transcriptomic and ChIP-seq data for *lin-15B*/LIN-15B.
(XLSX)

S4 Table. Comparative analysis of IPR genes and transcriptomic data for several SynMuv mutants.
(XLSX)

S5 Table. Yeast two-hybrid analysis of PALS-20 and PALS-25.
(XLSX)

S6 Table. List of strains used in this study.
(XLSX)

S7 Table. List of primers used in this study.
(XLSX)

Acknowledgments

We appreciate the helpful manuscript feedback from James Tirtorahardjo and Lakshmi Batachari. Strain MT2495 used in this study was provided by the *Caenorhabditis* Genetics Center (CGC), which is funded by the NIH Office of Research Infrastructure Programs (P40 OD010440).

Author contributions

Conceptualization: Malina A. Bakowski, Emily R. Troemel, Vladimir Lažetić.

Data curation: Ryan S. Underwood, Vladimir Lažetić.

Formal analysis: Eillen Tecle, Paaramitha Warushavithana, Samuel Li, Michael J. Blanchard, Crystal B. Chhan, Theresa Bui, Ryan S. Underwood, Malina A. Bakowski, Vladimir Lažetić.

Funding acquisition: Eillen Tecle, Emily R. Troemel, Vladimir Lažetić.

Investigation: Eillen Tecle, Paaramitha Warushavithana, Samuel Li, Michael J. Blanchard, Crystal B. Chhan, Theresa Bui, Vladimir Lažetić.

Methodology: Vladimir Lažetić.

Project administration: Emily R. Troemel, Vladimir Lažetić.

Resources: Vladimir Lažetić.

Supervision: Eillen Tecle, Vladimir Lažetić.

Validation: Paaramitha Warushavithana, Vladimir Lažetić.

Visualization: Paaramitha Warushavithana, Vladimir Lažetić.

Writing – original draft: Emily R. Troemel, Vladimir Lažetić.

Writing – review & editing: Eillen Tecle, Samuel Li, Michael J. Blanchard, Crystal B. Chhan, Emily R. Troemel, Vladimir Lažetić.

References

1. Li D, Wu M. Pattern recognition receptors in health and diseases. Signal Transduct Target Ther. 2021;6(1):291. https://doi.org/10.1038/s41392-021-00687-0 PMID: 34344870
2. Chen SN, Zou PF, Nie P. Retinoic acid-inducible gene I (RIG-I)-like receptors (RLRs) in fish: current knowledge and future perspectives. Immunology. 2017;151(1):16–25. https://doi.org/10.1111/imm.12714 PMID: 28109007
3. Dias Junior AG, Sampaio NG, Rehwinkel J. A Balancing Act: MDA5 in Antiviral Immunity and Autoinflammation. Trends Microbiol. 2019;27(1):75–85. https://doi.org/10.1016/j.tim.2018.08.007 PMID: 30201512
4. Rehwinkel J, Gack M. RIG-I-like receptors: their regulation and roles in RNA sensing. Nat Rev Immunol. 2020;20(9):537–51.
5. Ivashkiv LB, Donlin LT. Regulation of type I interferon responses. Nat Rev Immunol. 2014;14(1):36–49. https://doi.org/10.1038/nri3581 PMID: 24362405
6. Jadhav G, Teguh D, Kenny J, Tickner J, Xu J. Morc3 mutant mice exhibit reduced cortical area and thickness, accompanied by altered haematopoietic stem cells niche and bone cell differentiation. Sci Rep. 2016;6:25964. https://doi.org/10.1038/srep25964 PMID: 27188231
7. Lažetić V, Batachari LE, Russell AB, Troemel ER. Similarities in the induction of the intracellular pathogen response in Caenorhabditis elegans and the type I interferon response in mammals. Bioessays. 2023;45(11):e2300097. https://doi.org/10.1002/bies.202300097 PMID: 37667453
8. Mistry P, Kaplan MJ. Cell death in the pathogenesis of systemic lupus erythematosus and lupus nephritis. Clin Immunol. 2017;185:59–73. https://doi.org/10.1016/j.clim.2016.08.010 PMID: 27519955
9. Murimi-Worstell IB, Lin DH, Nab H, Kan HJ, Onasanya O, Tierce JC, et al. Association between organ damage and mortality in systemic lupus erythematosus: a systematic review and meta-analysis. BMJ Open. 2020;10(5):e031850. https://doi.org/10.1136/bmjopen-2019-031850 PMID: 32444429
10. Oikarinen M, Tauriainen S, Oikarinen S, Honkanen T, Collin P, Rantala I, et al. Type 1 diabetes is associated with enterovirus infection in gut mucosa. Diabetes. 2012;61(3):687–91. https://doi.org/10.2337/db11-1157 PMID: 22315304
11. Qaisar N, Jurczyk A, Wang JP. Potential role of type I interferon in the pathogenic process leading to type 1 diabetes. Curr Opin Endocrinol Diabetes Obes. 2018;25(2):94–100. https://doi.org/10.1097/MED.0000000000000399 PMID: 29369915
12. Uggetti C, La Piana R, Orcesi S, Egitto M, Crow Y, Fazzi E. Aicardi-Goutieres syndrome: neuroradiologic findings and follow-up. AJNR Am J Neuroradiol. 2009;30(10):1971–6.

13. Gaidt MM, Morrow A, Fairgrieve MR, Karr JP, Yosef N, Vance RE. Self-guarding of MORC3 enables virulence factor-triggered immunity. Nature. 2021;600(7887):138–42. https://doi.org/10.1038/s41586-021-04054-5 PMID: 34759314
14. Ding W, Smulan LJ, Hou NS, Taubert S, Watts JL, Walker AK. s-Adenosylmethionine Levels Govern Innate Immunity through Distinct Methylation-Dependent Pathways. Cell Metab. 2015;22(4):633–45. https://doi.org/10.1016/j.cmet.2015.07.013 PMID: 26321661
15. Zhou Y, Chen H, Zhong W, Tao YJ. Collagen and actin network mediate antiviral immunity against Orsay virus in C. elegans intestinal cells. PLoS Pathog. 2024;20(1):e1011366. https://doi.org/10.1371/journal.ppat.1011366 PMID: 38190406
16. Hu Y, Wang X, Song J, Wu J, Xu J, Chai Y, et al. Chromatin remodeler ARID1A binds IRF3 to selectively induce antiviral interferon production in macrophages. Cell Death Dis. 2021;12(8):743. https://doi.org/10.1038/s41419-021-04032-9 PMID: 34315861
17. Clapier CR, Iwasa J, Cairns BR, Peterson CL. Mechanisms of action and regulation of ATP-dependent chromatin-remodelling complexes. Nat Rev Mol Cell Biol. 2017;18(7):407–22. https://doi.org/10.1038/nrm.2017.26 PMID: 28512350
18. Tyagi M, Imam N, Verma K, Patel AK. Chromatin remodelers: We are the drivers!!. Nucleus. 2016;7(4):388–404. https://doi.org/10.1080/19491034.2016.1211217 PMID: 27429206
19. Chen K, Franz CJ, Jiang H, Jiang Y, Wang D. An evolutionarily conserved transcriptional response to viral infection in Caenorhabditis nematodes. BMC Genomics. 2017;18(1):303. https://doi.org/10.1186/s12864-017-3689-3 PMID: 28415971
20. Bakowski MA, Desjardins CA, Smelkinson MG, Dunbar TL, Lopez-Moyado IF, Rifkin SA, et al. Ubiquitin-mediated response to microsporidia and virus infection in C. elegans. PLoS Pathog. 2014;10(6):e1004200. https://doi.org/10.1371/journal.ppat.1004200 PMID: 24945527
21. Reddy K, Dror T, Sowa J, Panek J, Chen K, Lim E, et al. An intracellular pathogen response pathway promotes proteostasis in C. elegans. Current Biology. 2017;27(22):3544-53 e5.
22. Reddy KC, Dror T, Underwood RS, Osman GA, Elder CR, Desjardins CA, et al. Antagonistic paralogs control a switch between growth and pathogen resistance in C. elegans. PLoS Pathog. 2019;15(1):e1007528. https://doi.org/10.1371/journal.ppat.1007528 PMID: 30640956
23. Batachari LE, Dai AY, Troemel ER. Caenorhabditis elegans RIG-I-like receptor DRH-1 signals via CARDs to activate antiviral immunity in intestinal cells. Proc Natl Acad Sci U S A. 2024;121(29):e2402126121. https://doi.org/10.1073/pnas.2402126121 PMID: 38980902
24. Sowa JN, Jiang H, Somasundaram L, Tecle E, Xu G, Wang D. The Caenorhabditis elegans RIG-I Homolog DRH-1 Mediates the Intracellular Pathogen Response upon Viral Infection. Journal of Virology. 2020;94(2):e00100-19. https://doi.org/10.1128/JVI.00100-19
25. Batachari LE, Sarmiento MB, Wernet N, Troemel ER. Orsay Virus Infection in Caenorhabditis elegans. Curr Protoc. 2024;4(7):e1098. https://doi.org/10.1002/cpz1.1098 PMID: 38967546
26. Lažetić V, Blanchard MJ, Bui T, Troemel ER. Multiple pals gene modules control a balance between immunity and development in Caenorhabditis elegans. PLoS Pathog. 2023;19(7):e1011120. https://doi.org/10.1371/journal.ppat.1011120 PMID: 37463170
27. Gang SS, Grover M, Reddy KC, Raman D, Chang Y-T, Ekiert DC, et al. A pals-25 gain-of-function allele triggers systemic resistance against natural pathogens of C. elegans. PLoS Genet. 2022;18(10):e1010314. https://doi.org/10.1371/journal.pgen.1010314 PMID: 36191002
28. Gang SS, Lažetić V. Microsporidia: Pervasive natural pathogens of Caenorhabditis elegans and related nematodes. J Eukaryot Microbiol. 2024;71(5):e13027. https://doi.org/10.1111/jeu.13027 PMID: 38702921
29. Tecle E, Chhan CB, Franklin L, Underwood RS, Hanna-Rose W, Troemel ER. The purine nucleoside phosphorylase pnp-1 regulates epithelial cell resistance to infection in C. elegans. PLoS Pathog. 2021;17(4):e1009350. https://doi.org/10.1371/journal.ppat.1009350 PMID: 33878133
30. Lažetić V, Wu F, Cohen LB, Reddy KC, Chang Y-T, Gang SS, et al. The transcription factor ZIP-1 promotes resistance to intracellular infection in Caenorhabditis elegans. Nat Commun. 2022;13(1):17. https://doi.org/10.1038/s41467-021-27621-w PMID: 35013162
31. Rechtsteiner A, Ercan S, Takasaki T, Phippen TM, Egelhofer TA, Wang W, et al. The histone H3K36 methyltransferase MES-4 acts epigenetically to transmit the memory of germline gene expression to progeny. PLoS Genet. 2010;6(9):e1001091. https://doi.org/10.1371/journal.pgen.1001091 PMID: 20824077
32. Roussigne M, Kossida S, Lavigne A-C, Clouaire T, Ecochard V, Glories A, et al. The THAP domain: a novel protein motif with similarity to the DNA-binding domain of P element transposase. Trends Biochem Sci. 2003;28(2):66–9. https://doi.org/10.1016/S0968-0004(02)00013-0 PMID: 12575992

33. Gal C, Carelli FN, Appert A, Cerrato C, Huang N, Dong Y, et al. DREAM represses distinct targets by cooperating with different THAP domain proteins. Cell Rep. 2021;37(3):109835.

34. Tecle E, Troemel ER. Insights from C. elegans into Microsporidia Biology and Host-Pathogen Relationships. Exp Suppl. 2022;114:115–36. https://doi.org/10.1007/978-3-030-93306-7_5 PMID: 35544001

35. Samuelson AV, Klimczak RR, Thompson DB, Carr CE, Ruvkun G. Identification of Caenorhabditis elegans genes regulating longevity using enhanced RNAi-sensitive strains. Cold Spring Harb Symp Quant Biol. 2007;72:489–97. https://doi.org/10.1101/sqb.2007.72.068 PMID: 18419309

36. Petrella LN, Wang W, Spike CA, Rechtsteiner A, Reinke V, Strome S. synMuv B proteins antagonize germline fate in the intestine and ensure C. elegans survival. Development. 2011;138(6):1069–79. https://doi.org/10.1242/dev.059501 PMID: 21343362

37. Parker J, Palchaudhuri S, Yin H, Wei J, Chakravarti D. A transcriptional regulatory role of the THAP11-HCF-1 complex in colon cancer cell function. Molecular and Cellular Biology. 2012;32(9):1654–70.

38. Sabogal A, Lyubimov AY, Corn JE, Berger JM, Rio DC. THAP proteins target specific DNA sites through bipartite recognition of adjacent major and minor grooves. Nat Struct Mol Biol. 2010;17(1):117–23. https://doi.org/10.1038/nsmb.1742 PMID: 20010837

39. Ferguson EL, Horvitz HR. The multivulva phenotype of certain Caenorhabditis elegans mutants results from defects in two functionally redundant pathways. Genetics. 1989;123(1):109–21. https://doi.org/10.1093/genetics/123.1.109 PMID: 2806880

40. Polley SRG, Fay DS. A network of genes antagonistic to the LIN-35 retinoblastoma protein of Caenorhabditis elegans. Genetics. 2012;191(4):1367–80. https://doi.org/10.1534/genetics.112.140152 PMID: 22542970

41. Fay DS, Large E, Han M, Darland M. lin-35/Rb and ubc-18, an E2 ubiquitin-conjugating enzyme, function redundantly to control pharyngeal morphogenesis in C. elegans. Development. 2003;130(14):3319–30.

42. Bender AM, Kirienko NV, Olson SK, Esko JD, Fay DS. lin-35/Rb and the CoREST ortholog spr-1 coordinately regulate vulval morphogenesis and gonad development in C. elegans. Dev Biol. 2007;302(2):448–62. https://doi.org/10.1016/j.ydbio.2006.09.051 PMID: 17070797

43. Kirienko NV, Fay DS. Transcriptome profiling of the C. elegans Rb ortholog reveals diverse developmental roles. Dev Biol. 2007;305(2):674–84. https://doi.org/10.1016/j.ydbio.2007.02.021 PMID: 17368442

44. Kirienko NV, Mani K, Fay DS. Cancer models in Caenorhabditis elegans. Developmental Dynamics. 2010;239(5):1413–48.

45. Kudron M, Niu W, Lu Z, Wang G, Gerstein M, Snyder M, et al. Tissue-specific direct targets of Caenorhabditis elegans Rb/E2F dictate distinct somatic and germline programs. Genome Biol. 2013;14(1):R5. https://doi.org/10.1186/gb-2013-14-1-r5 PMID: 23347407

46. Wang D, Kennedy S, Conte D Jr, Kim JK, Gabel HW, Kamath RS, et al. Somatic misexpression of germline P granules and enhanced RNA interference in retinoblastoma pathway mutants. Nature. 2005;436(7050):593–7. https://doi.org/10.1038/nature04010 PMID: 16049496

47. Fay DS, Han M. The synthetic multivulval genes of C. elegans: functional redundancy, Ras-antagonism, and cell fate determination. Genesis. 2000;26(4):279–84. https://doi.org/10.1002/(sici)1526-968x(200004)26:4<279::aid-gene100>3.0.co;2-c PMID: 10748467

48. Fay DS, Yochem J. The SynMuv genes of Caenorhabditis elegans in vulval development and beyond. Dev Biol. 2007;306(1):1–9. https://doi.org/10.1016/j.ydbio.2007.03.016 PMID: 17434473

49. Mani K, Fay DS. A mechanistic basis for the coordinated regulation of pharyngeal morphogenesis in Caenorhabditis elegans by LIN-35/Rb and UBC-18-ARI-1. PLoS Genet. 2009;5(6):e1000510. https://doi.org/10.1371/journal.pgen.1000510 PMID: 19521497

50. Goetsch PD, Garrigues JM, Strome S. Loss of the Caenorhabditis elegans pocket protein LIN-35 reveals MuvB's innate function as the repressor of DREAM target genes. PLoS Genet. 2017;13(11):e1007088. https://doi.org/10.1371/journal.pgen.1007088 PMID: 29091720

51. Poulin G, Dong Y, Fraser AG, Hopper NA, Ahringer J. Chromatin regulation and sumoylation in the inhibition of Ras-induced vulval development in Caenorhabditis elegans. EMBO J. 2005;24(14):2613–23. https://doi.org/10.1038/sj.emboj.7600726 PMID: 15990876

52. Cox E, Hwang W, Uzoma I, Hu J, Guzzo CM, Jeong J, et al. Global Analysis of SUMO-Binding Proteins Identifies SUMOylation as a Key Regulator of the INO80 Chromatin Remodeling Complex. Mol Cell Proteomics. 2017;16(5):812–23. https://doi.org/10.1074/mcp.M116.063719 PMID: 28254775

53. Paakinaho V, Lempiäinen JK, Sigismondo G, Niskanen EA, Malinen M, Jääskeläinen T, et al. SUMOylation regulates the protein network and chromatin accessibility at glucocorticoid receptor-binding sites. Nucleic Acids Res. 2021;49(4):1951–71. https://doi.org/10.1093/nar/gkab032 PMID: 33524141

54. Ryu H-Y, Hochstrasser M. Histone sumoylation and chromatin dynamics. Nucleic Acids Res. 2021;49(11):6043–52. https://doi.org/10.1093/nar/gkab280 PMID: 33885816

55. Wotton D, Pemberton L, Merrill-Schools J. SUMO and chromatin remodeling. Advances in Experimental Medicine and Biology. 2017;963:35–50.

56. Pelisch F, Sonneville R, Pourkarimi E, Agostinho A, Blow JJ, Gartner A, et al. Dynamic SUMO modification regulates mitotic chromosome assembly and cell cycle progression in Caenorhabditis elegans. Nat Commun. 2014;5:5485. https://doi.org/10.1038/ncomms6485 PMID: 25475837

57. Pelisch F, Tammsalu T, Wang B, Jaffray EG, Gartner A, Hay RT. A SUMO-Dependent Protein Network Regulates Chromosome Congression during Oocyte Meiosis. Mol Cell. 2017;65(1):66–77. https://doi.org/10.1016/j.molcel.2016.11.001 PMID: 27939944

58. Walker DS, Ly S, Gower NJD, Baylis HA. IRI-1, a LIN-15B homologue, interacts with inositol-1,4,5-triphosphate receptors and regulates gonadogenesis, defecation, and pharyngeal pumping in Caenorhabditis elegans. Mol Biol Cell. 2004;15(7):3073–82. https://doi.org/10.1091/mbc.e04-01-0039 PMID: 15133127

59. Cockrum CS, Strome S. Maternal H3K36 and H3K27 HMTs protect germline development via regulation of the transcription factor LIN-15B. Elife. 2022;11.

60. Hoareau M, Rincheval-Arnold A, Gaumer S, Guenal I. DREAM a little dREAM of DRM: Model organisms and conservation of DREAM-like complexes: Model organisms uncover the mechanisms of DREAM-mediated transcription regulation. Bioessays. 2024;46(2):e2300125.

61. Sadasivam S, DeCaprio JA. The DREAM complex: master coordinator of cell cycle-dependent gene expression. Nat Rev Cancer. 2013;13(8):585–95. https://doi.org/10.1038/nrc3556 PMID: 23842645

62. Bender LB, Suh J, Carroll CR, Fong Y, Fingerman IM, Briggs SD, et al. MES-4: an autosome-associated histone methyltransferase that participates in silencing the X chromosomes in the C. elegans germ line. Development. 2006;133(19):3907–17. https://doi.org/10.1242/dev.02584 PMID: 16968818

63. Bannister AJ, Schneider R, Myers FA, Thorne AW, Crane-Robinson C, Kouzarides T. Spatial distribution of di- and tri-methyl lysine 36 of histone H3 at active genes. J Biol Chem. 2005;280(18):17732–6. https://doi.org/10.1074/jbc.M500796200 PMID: 15760899

64. Yuan W, Xu M, Huang C, Liu N, Chen S, Zhu B. H3K36 methylation antagonizes PRC2-mediated H3K27 methylation. J Biol Chem. 2011;286(10):7983–9. https://doi.org/10.1074/jbc.M110.194027 PMID: 21239496

65. Packer JS, Zhu Q, Huynh C, Sivaramakrishnan P, Preston E, Dueck H, et al. A lineage-resolved molecular atlas of C. elegans embryogenesis at single-cell resolution. Science. 2019;365(6459):eaax1971. https://doi.org/10.1126/science.aax1971 PMID: 31488706

66. Tabuchi TM, Rechtsteiner A, Strome S, Hagstrom KA. Opposing activities of DRM and MES-4 tune gene expression and X-chromosome repression in Caenorhabditis elegans germ cells. G3 (Bethesda). 2014;4(1):143–53. https://doi.org/10.1534/g3.113.007849 PMID: 24281426

67. Seetharaman A, Galagali H, Linarte E, Liu MHX, Cohen JD, Chetal K, et al. Decreased SynMuv B gene activity in response to viral infection leads to activation of the antiviral RNAi pathway in C. elegans. PLoS Biol. 2025;23(1):e3002748. https://doi.org/10.1371/journal.pbio.3002748 PMID: 39879188

68. Willis AR, Zhao W, Sukhdeo R, Wadi L, El Jarkass HT, Claycomb JM, et al. A parental transcriptional response to microsporidia infection induces inherited immunity in offspring. Sci Adv. 2021;7(19):eabf3114. https://doi.org/10.1126/sciadv.abf3114 PMID: 33952520

69. Rampazzo C, Ferraro P, Pontarin G, Fabris S, Reichard P, Bianchi V. Mitochondrial deoxyribonucleotides, pool sizes, synthesis, and regulation. J Biol Chem. 2004;279(17):17019–26. https://doi.org/10.1074/jbc.M313957200 PMID: 14747464

70. Cuomo CA, Desjardins CA, Bakowski MA, Goldberg J, Ma AT, Becnel JJ, et al. Microsporidian genome analysis reveals evolutionary strategies for obligate intracellular growth. Genome Res. 2012;22(12):2478–88. https://doi.org/10.1101/gr.142802.112 PMID: 22813931

71. Masaki T, Qu J, Cholewa-Waclaw J, Burr K, Raaum R, Rambukkana A. Reprogramming adult Schwann cells to stem cell-like cells by leprosy bacilli promotes dissemination of infection. Cell. 2013;152(1–2):51–67. https://doi.org/10.1016/j.cell.2012.12.014 PMID: 23332746

72. Kufer TA, Creagh EM, Bryant CE. Guardians of the Cell: Effector-Triggered Immunity Steers Mammalian Immune Defense. Trends Immunol. 2019;40(10):939–51. https://doi.org/10.1016/j.it.2019.08.001 PMID: 31500957

73. Song J, Win J, Tian M, Schornack S, Kaschani F, Ilyas M, et al. Apoplastic effectors secreted by two unrelated eukaryotic plant pathogens target the tomato defense protease Rcr3. Proc Natl Acad Sci U S A. 2009;106(5):1654–9. https://doi.org/10.1073/pnas.0809201106 PMID: 19171904

74. van der Hoorn RAL, Kamoun S. From Guard to Decoy: a new model for perception of plant pathogen effectors. Plant Cell. 2008;20(8):2009–17. https://doi.org/10.1105/tpc.108.060194 PMID: 18723576

75. Guan J, Tang L, Wang Y, Fu M, Xia T, Zheng K, et al. Microsporidian EnP1 alters host cell H2B monoubiquitination and prevents ferroptosis facilitating microsporidia survival. Proc Natl Acad Sci U S A. 2024;121(34):e2400657121. https://doi.org/10.1073/pnas.2400657121 PMID: 39141344

76. Ferrari R, Gou D, Jawdekar G, Johnson SA, Nava M, Su T, et al. Adenovirus small E1A employs the lysine acetylases p300/CBP and tumor suppressor Rb to repress select host genes and promote productive virus infection. Cell Host Microbe. 2014;16(5):663–76. https://doi.org/10.1016/j.chom.2014.10.004 PMID: 25525796

77. Wang X, Xia H, Liu S, Cao L, You F. Epigenetic regulation in antiviral innate immunity. Eur J Immunol. 2021;51(7):1641–51.

78. Ramirez-Carrozzi VR, Braas D, Bhatt DM, Cheng CS, Hong C, Doty KR, et al. A unifying model for the selective regulation of inducible transcription by CpG islands and nucleosome remodeling. Cell. 2009;138(1):114-28.

79. Zhang Q, Cao X. Epigenetic regulation of the innate immune response to infection. Nat Rev Immunol. 2019;19(7):417–32. https://doi.org/10.1038/s41577-019-0151-6 PMID: 30918351

80. Meng J, Liu X, Zhang P, Li D, Xu S, Zhou Q. Rb selectively inhibits innate IFN-beta production by enhancing deacetylation of IFN-beta promoter through HDAC1 and HDAC8. Journal of Autoimmunity. 2016;73:42–53.

81. Zhan X, Guo S, Li Y, Ran H, Huang H, Mi L, et al. Glioma stem-like cells evade interferon suppression through MBD3/NuRD complex-mediated STAT1 downregulation. J Exp Med. 2020;217(5).

82. Coustham V, Bedet C, Monier K, Schott S, Karali M, Palladino F. The C. elegans HP1 homologue HPL-2 and the LIN-13 zinc finger protein form a complex implicated in vulval development. Dev Biol. 2006;297(2):308–22. https://doi.org/10.1016/j.ydbio.2006.04.474 PMID: 16890929

83. Du L, Liu W, Rosen ST, Chen Y. Mechanism of SUMOylation-Mediated Regulation of Type I IFN Expression. J Mol Biol. 2023;435(5):167968. https://doi.org/10.1016/j.jmb.2023.167968 PMID: 36681180

84. Surana P, Gowda CM, Tripathi V, Broday L, Das R. Structural and functional analysis of SMO-1, the SUMO homolog in Caenorhabditis elegans. PLoS One. 2017;12(10):e0186622. https://doi.org/10.1371/journal.pone.0186622 PMID: 29045470

85. Fergin A, Boesch G, Greter NR, Berger S, Hajnal A. Tissue-specific inhibition of protein sumoylation uncovers diverse SUMO functions during C. elegans vulval development. PLoS Genet. 2022;18(6):e1009978. https://doi.org/10.1371/journal.pgen.1009978 PMID: 35666766

86. Costello ME, Petrella LN. C. elegans synMuv B proteins regulate spatial and temporal chromatin compaction during development. Development. 2019;146(19):dev174383. https://doi.org/10.1242/dev.174383 PMID: 31515206

87. Brenner S. The genetics of Caenorhabditis elegans. Genetics. 1974;77(1):71–94. https://doi.org/10.1093/genetics/77.1.71 PMID: 4366476

88. Emmons S, Klass M, Hirsh D. Analysis of the constancy of DNA sequences during development and evolution of the nematode Caenorhabditis elegans. Proceedings of the National Academy of Sciences of the United States of America. 1979;76(3):1333–7.

89. Kutscher L, Shaham S. Forward and reverse mutagenesis in C. elegans. WormBook. 2014:1–26.

90. Langmead B, Salzberg SL. Fast gapped-read alignment with Bowtie 2. Nat Methods. 2012;9(4):357–9. https://doi.org/10.1038/nmeth.1923 PMID: 22388286

91. Langmead B, Trapnell C, Pop M, Salzberg SL. Ultrafast and memory-efficient alignment of short DNA sequences to the human genome. Genome Biol. 2009;10(3):R25. https://doi.org/10.1186/gb-2009-10-3-r25 PMID: 19261174

92. Cingolani P, Patel VM, Coon M, Nguyen T, Land SJ, Ruden DM, et al. Using Drosophila melanogaster as a Model for Genotoxic Chemical Mutational Studies with a New Program, SnpSift. Front Genet. 2012;3:35. https://doi.org/10.3389/fgene.2012.00035 PMID: 22435069

93. Cingolani P, Platts A, Wang LL, Coon M, Nguyen T, Wang L, et al. A program for annotating and predicting the effects of single nucleotide polymorphisms, SnpEff: SNPs in the genome of Drosophila melanogaster strain w1118; iso-2; iso-3. Fly (Austin). 2012;6(2):80–92. https://doi.org/10.4161/fly.19695 PMID: 22728672

94. Ohnishi O. Spontaneous and ethyl methanesulfonate-induced mutations controlling viability in Drosophila melanogaster. II. Homozygous effect of polygenic mutations. Genetics. 1977;87(3):529–45. https://doi.org/10.1093/genetics/87.3.529 PMID: 200526

95. Schindelin J, Arganda-Carreras I, Frise E, Kaynig V, Longair M, Pietzsch T, et al. Fiji: an open-source platform for biological-image analysis. Nat Methods. 2012;9(7):676–82. https://doi.org/10.1038/nmeth.2019 PMID: 22743772

96. Rivera DE, Lazetic V, Troemel ER, Luallen RJ. RNA Fluorescence in situ Hybridization (FISH) to Visualize Microbial Colonization and Infection in Caenorhabditis elegans Intestines. Journal of Visualized Experiments. 2022;2022(185).

97. Wernet N, Tecle E, Sarmiento M, Kuo C-J, Chhan C, Baick I, et al. Adenosine deaminase and deoxyadenosine regulate intracellular immune response in C. elegans. iScience. 2025;2025:111950.

98. Timmons L, Fire A. Specific interference by ingested dsRNA. Nature. 1998;395(6705):854. https://doi.org/10.1038/27579 PMID: 9804418

99. Fromont-Racine M, Rain JC, Legrain P. Toward a functional analysis of the yeast genome through exhaustive two-hybrid screens. Nat Genet. 1997;16(3):277–82. https://doi.org/10.1038/ng0797-277 PMID: 9207794

100. Formstecher E, Aresta S, Collura V, Hamburger A, Meil A, Trehin A, et al. Protein interaction mapping: a Drosophila case study. Genome Res. 2005;15(3):376–84. https://doi.org/10.1101/gr.2659105 PMID: 15710747